CellPress

Cell Host & Microbe
Article

Convergent Targeting of a Common Host Protein-Network by Pathogen Effectors from Three Kingdoms of Life

Ralf Weßling,[1,18] Petra Epple,[2,14,18] Stefan Altmann,[3,18] Yijian He,[2,15,18] Li Yang,[2,18] Stefan R. Henz,[4] Nathan McDonald,[2] Kristin Wiley,[2] Kai Christian Bader,[5] Christine Gläßer,[5,16] M. Shahid Mukhtar,[2,6] Sabine Haigis,[1] Lila Ghamsari,[7,17] Amber E. Stephens,[1] Joseph R. Ecker,[8] Marc Vidal,[7] Jonathan D.G. Jones,[9] Klaus F.X. Mayer,[5] Emiel Ver Loren van Themaat,[1] Detlef Weigel,[4] Paul Schulze-Lefert,[1] Jeffery L. Dangl,[2,10,11,12,*] Ralph Panstruga,[1,13,*] and Pascal Braun[3,*]

[1]Department of Plant Microbe Interactions, Max Planck Institute for Plant Breeding Research, Cologne, D-50829, Germany
[2]Howard Hughes Medical Institute and Department of Biology, University of North Carolina at Chapel Hill, Chapel Hill, NC 27599, USA
[3]Technische Universität München (TUM), Center for Life and Food Sciences Weihenstephan, Department for Plant Systems Biology, D-85354 Freising, Germany
[4]Department of Molecular Biology, Max Planck Institute for Developmental Biology, D-72076 Tübingen, Germany
[5]Plant Genome and Systems Biology, Helmholtz Zentrum München, D-85764 Neuherberg, Germany
[6]Department of Biology, University of Alabama Birmingham, Birmingham, AL 35294, USA
[7]Center for Cancer Systems Biology (CCSB) and Department of Cancer Biology, Dana Farber Cancer Institute, and Harvard Medical School, Department of Genetics, Boston, MA 02215, USA
[8]Howard Hughes Medical Institute and Salk Institute for Biological Studies, Plant Biology Lab, La Jolla, CA 92037, USA
[9]The Sainsbury Laboratory, John Innes Centre, Norwich Research Park, Colney Lane, Norwich NR4 7UH, UK
[10]Curriculum in Genetics and Molecular Biology, University of North Carolina at Chapel Hill, Chapel Hill, NC 27599, USA
[11]Carolina Center for Genome Science, University of North Carolina at Chapel Hill, Chapel Hill, NC 27599, USA
[12]Department of Microbiology and Immunology, University of North Carolina at Chapel Hill, Chapel Hill, NC 27599, USA
[13]Rheinisch Westfälische Technische Hochschule (RWTH) Aachen University, Institute for Biology I, Unit of Plant Molecular Cell Biology, D-52074 Aachen, Germany
[14]Present address: BASF Plant Science LP, Research Triangle Park, NC 27709, USA
[15]Present address: Department of Plant Pathology, NC State University, Raleigh, NC 27695, USA
[16]Present address: Zentrum für Molekulare Biologie der Universität Heidelberg, D-69120 Heidelberg, Germany
[17]Present address: Department of Systems Biology, Columbia University, New York, NY 10032, USA
[18]Co-first Authors
*Correspondence: dangl@email.unc.edu (J.L.D.), panstruga@bio1.rwth-aachen.de (R.P.), pbraun@wzw.tum.de (P.B.)
http://dx.doi.org/10.1016/j.chom.2014.08.004

SUMMARY

While conceptual principles governing plant immunity are becoming clear, its systems-level organization and the evolutionary dynamic of the host-pathogen interface are still obscure. We generated a systematic protein-protein interaction network of virulence effectors from the ascomycete pathogen *Golovinomyces orontii* and *Arabidopsis thaliana* host proteins. We combined this data set with corresponding data for the eubacterial pathogen *Pseudomonas syringae* and the oomycete pathogen *Hyaloperonospora arabidopsidis*. The resulting network identifies host proteins onto which intraspecies and interspecies pathogen effectors converge. Phenotyping of 124 *Arabidopsis* effector-interactor mutants revealed a correlation between intraspecies and interspecies convergence and several altered immune response phenotypes. Several effectors and the most heavily targeted host protein colocalized in subnuclear foci. Products of adaptively selected *Arabidopsis* genes are enriched for interactions with effector targets. Our data suggest the existence of a molecular host-pathogen interface that is conserved across *Arabidopsis* accessions, while evolutionary adaptation occurs in the immediate network neighborhood of effector targets.

INTRODUCTION

The spread of pathogens is predicted to change in the wake of global warming, generating emerging epidemics threatening human welfare and security. Plants evolved a sophisticated two-layered defense system to detect and defend against the majority of potential pathogens (Chisholm et al., 2006; Dodds and Rathjen, 2010; Jones and Dangl, 2006). Activation of plant pattern-recognition receptor kinases by highly conserved microbe-associated molecular patterns (MAMPs) triggers a complex cellular response termed MAMP-triggered immunity (MTI) that can stop microbial proliferation. Host-adapted pathogens are equipped with diverse suites of virulence effectors, which are delivered into the plant cell by various and mostly poorly understood means. Effector proteins interact with host proteins to undermine MTI and to modify host physiology, thus

enhancing pathogen proliferation (Feng and Zhou, 2012; Raffaele and Kamoun, 2012; Win et al., 2012). Plants evolved highly polymorphic intracellular nucleotide-binding site, leucine-rich repeat (NLR) proteins to recognize intracellular effectors. Activation of NLRs is also poorly understood in all but a few cases, but it can proceed by either direct effector-NLR interaction or upon effector modification of an NLR-associated host target protein. NLR activation results essentially in a more rapid and higher amplitude MTI output known as effector-triggered immunity (Chisholm et al., 2006; Dodds and Rathjen, 2010; Jones and Dangl, 2006).

While the conceptual principles of the plant immune system have been elucidated, knowledge of its systems-level organization and the evolutionary dynamic of the molecular host-pathogen interface are rudimentary. Filling this gap represents an important goal in the quest for targeted crop improvement (Dangl et al., 2013; Pardey et al., 2013). The reference eudicot *Arabidopsis thaliana* (hereafter *Arabidopsis*) is host to a range of evolutionarily diverse pathogens, including bacteria, oomycetes, and fungi. We defined an effector-host network featuring protein interactions between effectors from the oomycete *Hyaloperonospora arabidopsidis* (*Hpa*) and the eubacterium *Pseudomonas syringae* (*Psy*) and 8,000 *Arabidopsis* host proteins and integrated this with a first-generation *Arabidopsis* interactome map (Consortium, 2011; Mukhtar et al., 2011). Our results suggested that effectors from these evolutionarily diverse pathogens converge onto common host proteins, which were characterized by a high interaction degree and a central position in the host protein network. Immune function was demonstrated for 15 of 17 tested proteins that are effector targets shared by both pathogens (Mukhtar et al., 2011). It remained to be determined whether the effector convergence onto common targets extended to *Arabidopsis* pathogens from other kingdoms from the microbial tree of life, how effector convergence related broadly to phenotypic relevance, and how the central network position of many targeted host proteins accommodated the selective pressure imposed by pathogens.

While the effector set of facultative phytopathogenic bacteria like *Psy* is confined to 10–40 effectors per strain (Baltrus et al., 2011), the genomes of eukaryote obligate biotrophic plant pathogens encode extensive apparent effector arsenals (Baxter et al., 2010; Raffaele and Kamoun, 2012; Win et al., 2012). Only a minute fraction of these are functionally characterized, largely because genetic screens are challenging or as yet impossible in most of these organisms. The increased availability of genome sequences and improved bioinformatic prediction pipelines facilitate identification of proteins carrying signatures of virulence effectors. Recent additions include the powdery mildew fungi, an economically important class of plant pathogens with annotated candidate effector repertoires in several species, strains, and *formae speciales* (Hacquard et al., 2013; Pedersen et al., 2012; Wicker et al., 2013). The obligate biotrophic ascomycete *Golovinomyces orontii* (*Gor*) causes powdery mildew on *Arabidopsis* (Micali et al., 2008). The available genome resources make *Gor* an excellent pathogen to identify effectors and their interacting host proteins. Additionally, this ascomycete belongs to a different taxonomic kingdom than the eubacterium *Psy* and the stramenopile *Hpa* (Figure 1A), providing an evolutionary contrast from which to challenge the principles we previously proposed regarding the structure of a plant-pathogen interactome network (Mukhtar et al., 2011).

RESULTS

Definition and Cloning of Candidate *Golovinomyces orontii* Virulence Effectors

We identified *Gor* effector candidates (*OECs*) iteratively using a bioinformatic pipeline (Figure 1B). Using several criteria, including a size cutoff; presence of an N-terminal secretion signal; and, due to the rapidly evolving nature of effectors, a lack of homology outside the powdery mildew fungi; we predicted 103 *OECs* de novo from a sequenced haustorial *Gor* cDNA library (Weßling et al., 2012). This set of *OECs*, and candidate effector sequences from the barley powdery mildew *Blumeria graminis* f. sp. *hordei* (*Bgh*) were then used as templates for iterative homology searches in the same haustorial cDNA library (Pedersen et al., 2012; Weßling et al., 2012). These iterations identified two and ten additional *OECs*, respectively, yielding a total of 115 *OECs*. Sequence relatedness among *Gor* effectors was usually low (Figure 1B). Sequences with similarity to *OECs* were rare in the *Bgh* genome but frequent in the genome of the pea powdery mildew *Erysiphe pisi* (Figure 1B). This pattern is consistent with the different evolutionary distances between *Gor* and the two other powdery mildew species and suggests that conserved effectors may constitute elements of a putative powdery mildew core effector set. We subsequently cloned the open reading frames (ORFs) of mature OECs without signal peptides into Gateway Entry vectors and verified the identity of 84 full-length *OECs* clones (73% success rate) (Table S1 available online).

Systematic Host-Protein Interactome Mapping Using the *G. orontii* Effector Candidates

We defined protein-protein interactions between 69 OECs and 12,000 *Arabidopsis* proteins encoded by sequence-verified ORFs (12k_space) (15 of the 84 OECs autoactivated and were not screened). A subset of 8,000 ORFs (8k_space) was previously used to generate the *Arabidopsis* Interactome 1 (AI-1) and the Plant-Pathogen Immune Network 1 (PPIN-1) (Consortium, 2011; Mukhtar et al., 2011). We used a stringent Y2H mapping pipeline, which yields high-quality data with a low false-discovery rate (Braun, 2012; Dreze et al., 2010) (Figure 1C), to assemble a *Gor* effector-host interactome network (*Gor*_EHIn$_{12k}$) (Figure S1; Table S1). The subset of interactions of OECs with host-proteins within the previously screened 8k_space is denoted *Gor*_EHIn$_{8k}$ (Figure S1). In *Gor*_EHIn$_{12k}$, we found, on average, 2.3 interaction partners for positive OECs (Figure 1E); 38 OECs yielded no interactor. Conversely, 16 host proteins interacted with multiple, typically phylogenetically unrelated, OECs (Figures 1D and S1C). This new data set allowed us to consider whether the host interactors of OECs included previously observed interactors of oomycete and bacterial effectors and whether the convergence previously observed for *Psy* and *Hpa* extended to the *Gor* effector host network.

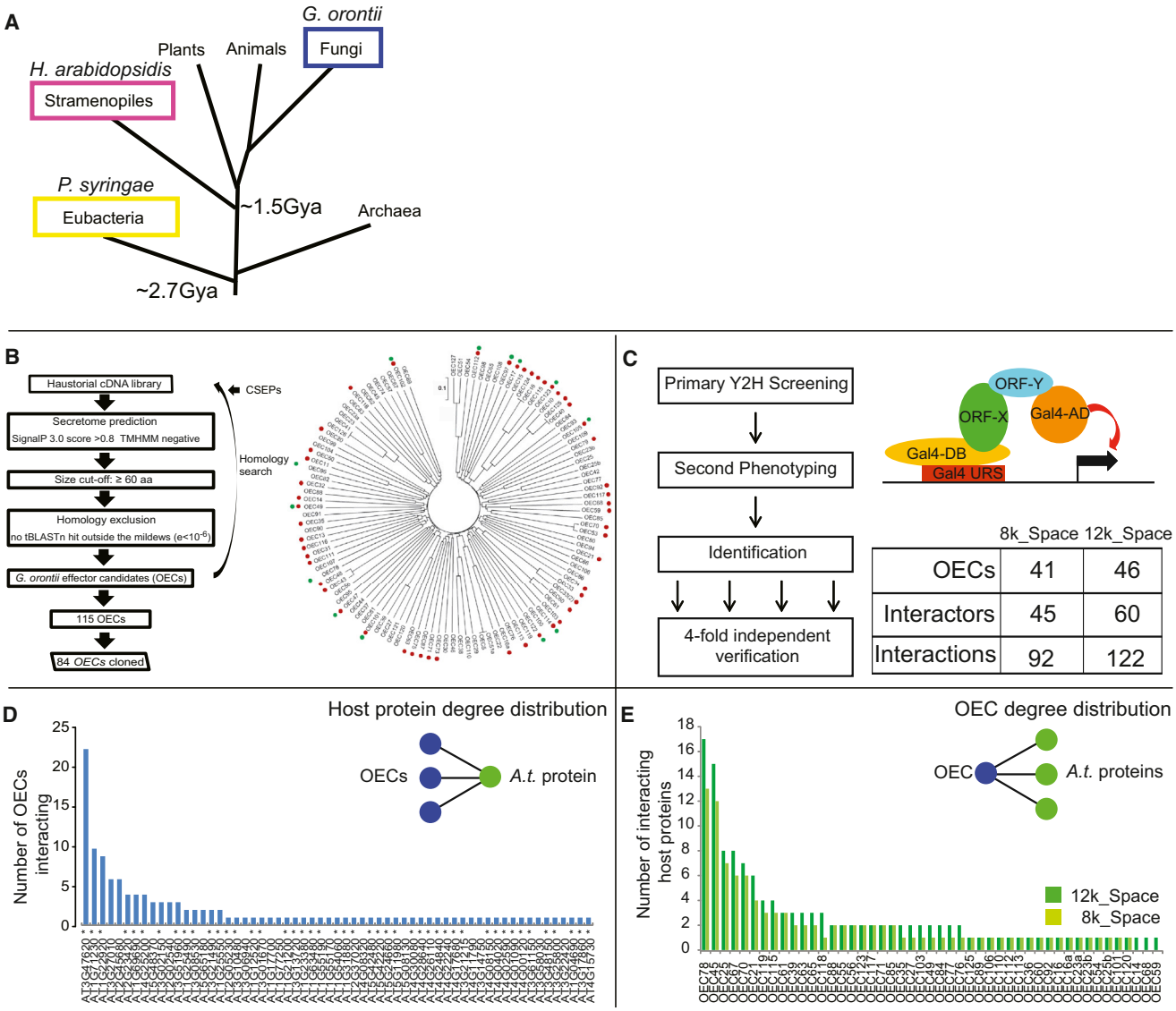

Figure 1. *Gor* Effector Identification and Interactome Mapping

(A) *Golovinomyces orontii* is a pathogenic ascomycete that diverged approximately 2.7 and 1.5 billion years ago (Gya), respectively, from the other *Arabidopsis* pathogens (Kemen and Jones, 2012; Markow, 2005).

(B) Effector identification pipeline and family relationships of identified and cloned *OECs* and the presence of homologs in the powdery mildews *Blumeria graminis* f. sp. *hordei* (green dots) and *Erysiphe pisi* (red dots).

(C) Our Y2H pipeline consists of three interrogation steps: screening, phenotyping, and 4-fold verification, resulting in the indicated number of interactions.

(D) Degree distribution of *Arabidopsis* proteins interacting with OECs. Asterisks indicate 8k_space proteins.

(E) Degree distribution of OECs interacting with *Arabidopsis* proteins in the 8k_space (light green) and 12K_space (dark green). See also Figure S1 and Table S1.

Integrated Network Map Reveals Interspecies Effector Convergence onto Shared Host Proteins

The interactions of effectors from all three pathogens (*Gor*, *Hpa*, and *Psy*) with host proteins were integrated with interactions among host proteins from AI-1, PPIN-1, and the literature to yield a comprehensive Plant-Pathogen Immune Network 2 (PPIN-2) (Figure S2; Table S1). To generate a network produced with identical experimental parameters, effector interactions with the *Arabidopsis* 8k_space proteins were extracted and integrated with their mutual interactions from the systematic AI-1_{MAIN} data set to yield PPIN-2_{8k_sys} (Figure 2A; Table S1). PPIN-2_{8k_sys} consists of 178 *Arabidopsis* host proteins and 123 effectors connected by 421 effector host-protein interactions and 162 interactions among host proteins (Figure S1B). PPIN-2_{8k_sys} was used for all subsequent statistical analyses unless otherwise noted. An overview describing the different data sets is provided in Figure S1.

One large cluster was apparent within PPIN-2_{8k_sys} in which 88 of the 178 effector-interactors (49%) are connected to each other by AI-1_{MAIN} interactions (Figure 2A). Eighty-six effector-interacting host proteins did not interact with any other effector-interactor in AI-1_{MAIN}, although some were connected

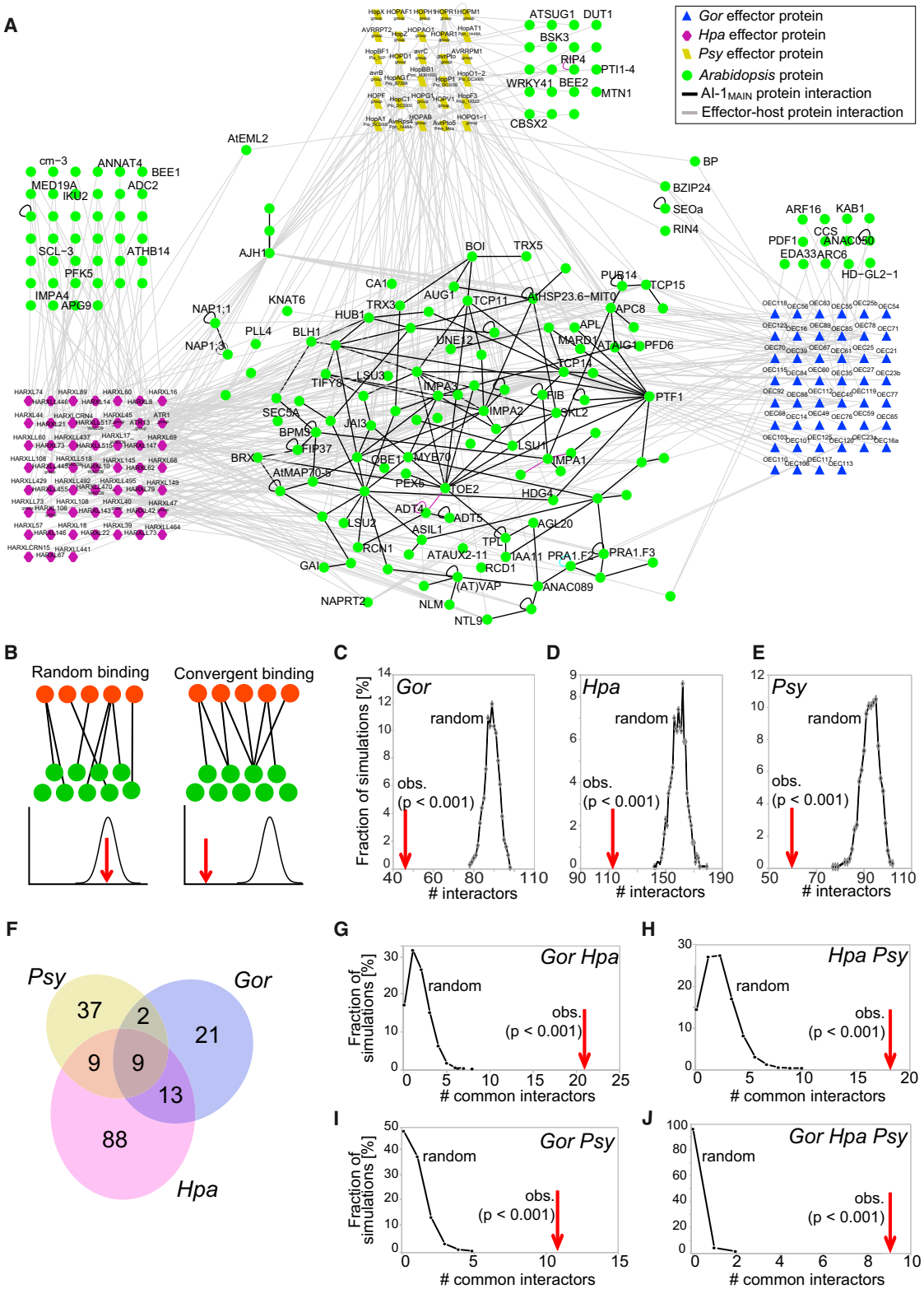

Figure 2. Network Integration

(A) The integrated PPIN-2_{8k_sys} network of host proteins interacting with *Gor*, *Hpa*, and *Psy* effectors and physical interactions among host proteins derived from AI-1_{MAIN} in the 8k_space.

(B) Random and convergent interaction of *Arabidopsis* proteins (green) with effectors (red) can be distinguished by degree-preserving random network rewiring and simulation.

(legend continued on next page)

by interactions from other data sets (e.g., PPIN-1 or literature data) (Figure S2A). Degree-preserving random network rewiring revealed that the effector-interactors were less connected to each other in AI-1_{MAIN} than expected by chance (exp. $p < 0.001$; Figure S2B). This finding may indicate that effectors collectively target different parts of the overall network rather than a functionally coherent subnetwork.

Gene ontology (GO) enrichment analysis on TAIR10 annotations of effector targets returned mostly high-level categories of regulatory processes (Table S2), including defense signaling, potentially due to our previous data being incorporated into the TAIR annotation. We focused on specific, and hence more informative, GO terms that annotate less than 100 genes in AI-1_{MAIN} and found terms related to development (e.g., floral organ development), auxin- and salicylic-acid-mediated signaling, and others (p value 0.005; Table S2). Both of these phytohormones play important roles in plant pathogen interactions (Robert-Seilaniantz et al., 2011). The functional categories are consistent with analysis of specific bacterial effectors and their targets (Deslandes and Rivas, 2012; Win et al., 2012).

To evaluate whether the apparent OEC convergence onto common host proteins (Figure 1D) was significant, we simulated OECs randomly interacting with AI-1_{MAIN} proteins. The frequency distribution of the randomly observed values obtained in these simulations was used to calculate an experimental p value for OEC interactions with host proteins (Figure 2B). We performed 10,000 simulations with all proteins in the AI-1_{MAIN} network represented according to their degree in AI-1_{MAIN}. The mean random expectation of more than 80 OEC-interacting proteins is significantly higher than the experimentally observed value of 45 *Arabidopsis* proteins interacting with OECs in $EHIn_{8k\_sys}$ (Figure 2C; exp. p value < 0.0001). Thus, OEC effectors converge onto a small set of host proteins. We refer to the convergence of effectors from a single pathogen species onto common host proteins as "intraspecies convergence." Applying this analysis to *Hpa* and *Psy* effectors revealed the same striking and significant intraspecies convergence as observed for OECs (Figures 2D and 2E; exp. p value < 0.0001). Thus, effectors of pathogens from diverse kingdoms exhibit intraspecies convergence onto host proteins.

We previously observed convergence of the combined *Psy* and *Hpa* effector sets onto common host proteins ("interspecies convergence"), several of which were hubs (highly interconnected host proteins) (Mukhtar et al., 2011). The *Gor*_EHIn data enabled us to extend the finding of convergence to a divergent fungal pathogen. Effectors from the three pathogens exhibited remarkable overlap with regard to shared host-interacting proteins within $EHIn_{8k\_sys}$; this included 24 host proteins interacting with effectors from two pathogens and nine host proteins interacting with effectors from all three (Figure 2F). We performed simulations for all pairwise, and the three-fold, combinations of the three pathogens. In each case, the experimentally observed overlap was significantly higher than expected by chance (Figures 2G–2H; exp. p value < 0.0001).

Thus, we observed significant intraspecies and interspecies convergence of effectors from three evolutionarily highly diverse (hemi-)biotrophic pathogens. This strongly suggests that the convergence is the product of natural selection and that the respective host proteins are functionally relevant to the pathogen.

Genetic Support for Effector-Interactors: Altered Infection Phenotypes

We tested the functional relevance of 124 effector-interacting host proteins in PPIN-2_{8k_sys} using available transfer DNA (T-DNA) insertion mutants (Alonso and Ecker, 2006). We focused on exon insertions early in genes and tested independent alleles when available (Table S3). We confirmed by PCR both T-DNA insertion into the gene of interest and homozygosity for a total of 179 T-DNA lines. We did not confirm each line as an mRNA null, leaving the formal possibility of phenotypic false negatives. These validated mutants were phenotyped using the *Gor* isolate MPIPZ (Spanu et al., 2010), which is virulent on the Col-0 genetic background of the mutants (Micali et al., 2008; Weßling et al., 2012); *Psy* strain *Pto* DC3000, also virulent on Col-0; and three *Hpa* isolates: Emwa1, Emoy2, and Noco2. The *Hpa* isolates Emwa1 and Emoy2 are avirulent on Col-0 due to RPP4-mediated recognition, whereas *Hpa* Noco2 is virulent on Col-0 (van der Biezen et al., 2002). The *Hpa* isolates were selected to detect both enhanced disease susceptibility (*eds*) and enhanced disease resistance (*edr*) phenotypes.

At least one altered infection phenotype was detected for 63 of the 124 tested effector-interactors (51% validation rate) (Figures 3A, 3B, and S3; Table S3). The 63 interactors with infection phenotypes will be referred to as effector *targets*. Of these, 25 (40%) demonstrated exclusively *eds* phenotypes upon pathogen challenge, indicating that the corresponding wild-type proteins function in immune responses. Mutants for 21 targets (33%) exhibited exclusively *edr* phenotypes upon pathogen challenge, most pronounced in response to the virulent *Hpa* isolate Noco2. These host proteins may facilitate pathogen sustenance in the host. Alternatively, they may repress an activator of immune signaling, a function possibly stabilized by the interacting virulence effectors; thus, in the absence of the putative negative regulator, effector action is neutralized and host resistance increases. We noted divergent disease phenotypes for 17 (27%) effector targets; these are cases where mutants exhibited an *edr* phenotype with one pathogen or *Hpa* isolate and an *eds*

(C) Random interactors observed in degree-preserving network rewiring simulations of *Gor* effector-host protein interactions versus observed value.
(D) As in (C), but for *Hpa* effector-target interactions.
(E) As in (C), but for *Psy* effector-host protein interactions.
(F) Venn diagram showing observed overlap between effector-interactors from the three pathogens.
(G) Simulated random and observed overlap between *Gor* and *Hpa* effector-interactors.
(H) As in (G), but between *Hpa* and *Psy* effector-interactors.
(I) As in (G), but between *Gor* and *Psy* effector-interactors.
(J) As in (G), but between *Gor*, *Hpa*, and *Psy* effector-interactors. In (C)–(E) and (G)–(J), random simulations are shown by black lines and observed values are highlighted by red arrows. See also Figure S2 and Table S1.

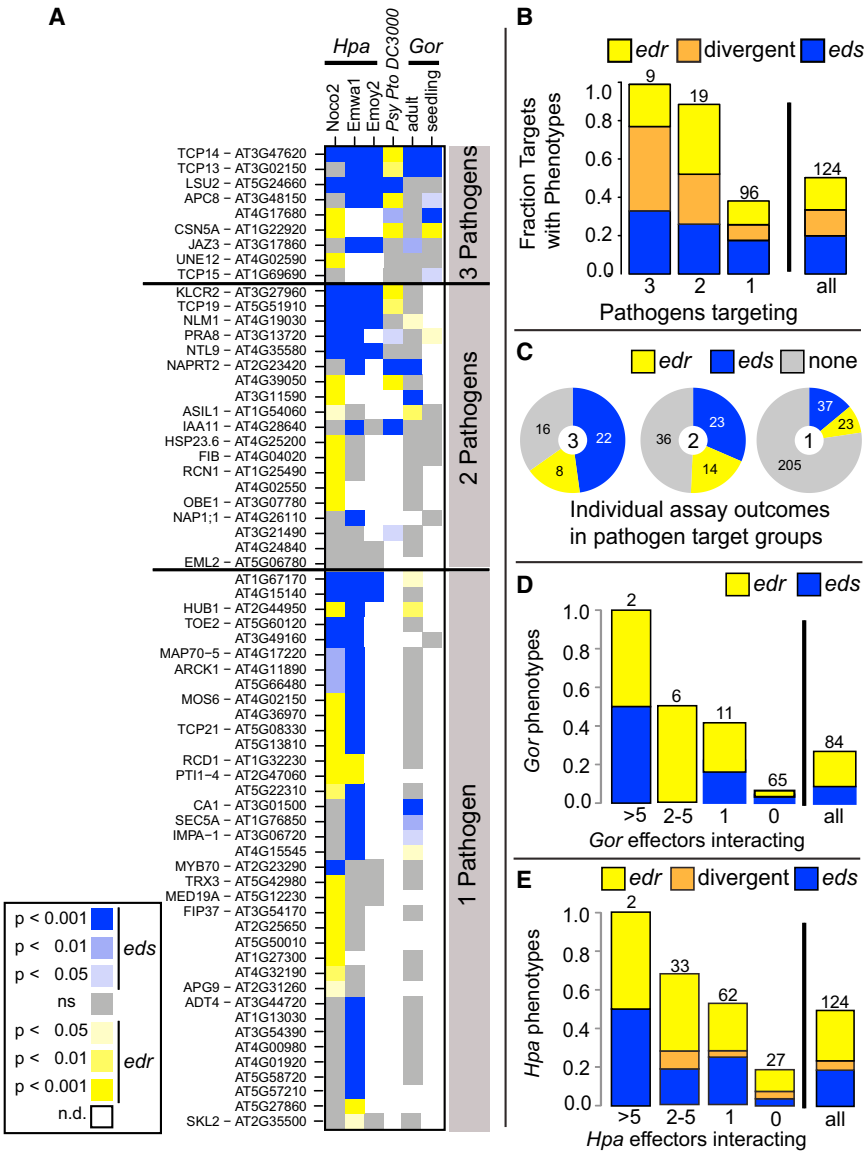

Figure 3. Phenotypic Characterization of Effector-Interactor Mutants

(A) Heatmap summarizing the outcome of phenotypic analyses of mutants in genes encoding the indicated effector-interactors in infection assays with the noted pathogens and developmental stages. Host proteins are sorted by the number of pathogens interacting with them, then by number of observed phenotypes and performed assays. Mutant lines for 59 proteins interacting with effectors from a single pathogen did not show any disease phenotype and are not shown. Refer to Table S3 for raw data for all phenotyped loci and Figure S3 for complete results for all tested lines.

(B) Fraction of mutant lines for proteins interacting with effectors from the indicated number of pathogens that exhibited an *edr*, *eds*, or divergent phenotypes across the assays.

(C) Pie chart representation of the phenotype density; the number of observed phenotypes relative to individual assays performed for that group. Each pie displays data for proteins that interacted with effectors from the number of pathogens given in the center.

(D) Fraction of mutant lines for proteins targeted by the indicated number of *Gor* effectors for which *edr* or *eds* phenotypes were observed. Numbers above bars indicate the number of targets in that class.

(E) As in (D), but for proteins targeted by the indicated number of *Hpa* effectors for which *edr* or *eds* phenotypes were observed. Numbers above bars indicate the number of effector-interactors in the class.

phenotype with a second pathogen or a different *Hpa* isolate, as described in Pieterse et al., (2012). Their existence suggests that these host proteins may have disease-specific functions. The TCP transcription factors TCP13, TCP14, and TCP19, whose mutants exhibited *eds* phenotypes with the biotrophic pathogens *Hpa* and *Gor*, but *edr* phenotypes with the hemibiotrophic *Psy*, are particularly interesting in this context.

Effector Convergence Correlates with Altered Infection Phenotypes

The nonrandom nature of effector-host protein connectivity suggested that the network topology of the plant immune system is the product of natural selection and, consequently, that the convergence we observed is biologically meaningful. We explored whether a relationship exists between intraspecies and interspecies effector convergence and altered pathogen infection phenotypes. A host protein was considered a point of intraspecies convergence when at least two effectors from the same pathogen interacted with it and an object of interspecies convergence when effectors from different pathogens interacted with it.

Effector-interactors were binned by whether they interacted with effectors from three, two, or one pathogen(s) (Figure 2F). The rate of altered infection-related phenotypes was evaluated for each bin and compared to the overall rate ("all" column) (Figure 3B). We noted a positive correlation between the degree of interspecies convergence and the probability of observing an infection phenotype in that bin (Figure 3B). To exclude that our observation was due to deeper phenotypic interrogation of the most highly targeted proteins, we also calculated the phenotype density for proteins interacting with effectors from three, two, or one pathogen as the fraction of assays (individual squares in Figure 3B) in which an *edr* or *eds* phenotype was observed divided by the total number of assays performed in this group. This analysis confirmed the correlation between convergence and phenotypic relevance of the targeted host protein (Figure 3C).

We then evaluated the phenotypic relevance of genes encoding host proteins that are objects of intraspecies convergence (Figures 2C–2E). We binned host proteins according to the number of effectors from each pathogen interacting with them and evaluated how often an altered immunity phenotype could be observed with the respective pathogen. We found *edr* or *eds*

phenotypes for all mutants in genes encoding the proteins targeted by more than five *Gor* or *Hpa* effectors (Figures 3D and 3E). The fraction of phenotypically validated host targets decreased proportional to the degree at which effectors are connected to the respective plant proteins (Figures 3D and 3E). Thus, the extent of intraspecies effector convergence onto host targets is also directly correlated to the functional relevance of the targeted proteins.

We wondered whether the host proteins that interact with effectors from multiple pathogens were also targeted repeatedly by the suite of effectors from any individual pathogen. All nine *Arabidopsis* proteins targeted by effectors from all three pathogens are also intraspecies convergence points for at least one pathogen (Figure S3). Furthermore, 16 of 23 proteins targeted by effectors from two pathogens are also points of intraspecies convergence. Thus, the most commonly targeted *Arabidopsis* proteins are objects of both intraspecies and interspecies effector convergence (Fisher's exact test, $p < 0.001$).

Effector convergence is exemplified by TCP14, a member of a large family of transcriptional regulators typically recognized to function in plant development (Martín-Trillo and Cubas, 2010). TCP14 was the most targeted host protein, interacting with 23 distinct OECs, 25 *Hpa* effectors, and four *Psy* effectors and exhibiting disease phenotypes in all assays (Figure 3A). The related family members TCP13, TCP15, and TCP19 were also targeted multiple times by effectors from at least two pathogens and exhibited altered infection phenotypes. These findings suggest an important and possibly universal role of this class of TFs during infection, consistent with their emerging role as targets of phytoplasma effectors (Sugio et al., 2011) and the recent demonstration of their importance in plant immunity (Kim et al., 2014).

Effectors Colocalize with TCP14 In Planta

To independently validate the convergence concept using cell biological methods, we tested TCP14 for colocalization with 11 of the 25 interacting *Hpa* effectors, focusing on those effectors demonstrated to localize to the nucleus (Caillaud et al., 2012), 19 of the 23 *Gor* effectors not previously localized, and three of four *Psy* effectors (Table S4).

TCP14 localized to subnuclear foci in transgenic *Arabidopsis* plants expressing a functional TCP14-YFP fusion (Figure S4). We used this knowledge to develop a transient overexpression assay platform in *Nicotiana benthamiana* where TCP14-RFP was also localized to subnuclear foci (Figure 4A). Under these conditions, TCP14-RFP did not colocalize with a wide set of controls with which it did not interact in Y2H: free YFP (Figure 4B), representative effectors (HopBC1, HaRxL62, and OEC56), an unrelated TF (bZIP5), or an unrelated, subnuclear body-localized protein (PhyB) (Chen et al., 2005) (Figure S4). We then demonstrated that TCP14 can relocalize into subnuclear foci 64% and 74% of the tested *Hpa* and *Gor* effectors, respectively, and one of three *Psy* effectors (Figures 4C and S4). Thus, the majority (67%) of tested interactions between effectors and TCP14 were validated by relocalization in vivo (Table S4). We confirmed these findings via coimmunoprecipitation for single effectors from each pathogen (Figure 4D). We thus validated in planta the majority of effector interactions with the most heavily targeted host protein, TCP14, consistent with our claim that the observed convergence onto the plant protein is not an artifact.

Proteins Interacting with Common Effector Targets Are Likely under Positive Selection

We sought evidence for the evolutionary relevance of our effector targets from population genomics. We used the complete genomes of 80 accessions sequenced in the context of the 1001 Genomes project and mapped on the Col-0 reference genome (Cao et al., 2011). These were collected in eight regions distributed over Europe and Asia, where *Arabidopsis* naturally occurs, and thus provide a large spatial and phylogenetic sample of genotypes adapted to different environments (http://1001genomes.org/data/). For all proteins in AI-1_{MAIN}, we calculated Tajima's D (D_T) and Watterson's estimator θ (θ_W) to assess the allele frequency deviation from neutrality and scaled mutation rate, respectively (Tajima, 1989; Watterson, 1975) (Table S5). As the two statistics lead to different ordered gene rankings, we also built a consensus ranking based on the relative positions of each gene in the two ranked lists (Dθ-ranking). In addition, we constructed consensus protein sequences from 81 *Arabidopsis* accessions (80 plus the Col-0 reference) by majority voting (S.A., K.C.B., K.F.X.M., and P.B., unpublished data) and used this resource to identify SNPs that give rise to altered amino acid sequences (amino acid polymorphisms [AAPs]) in the 2,653 AI-1_{MAIN} proteins (Table S5).

We asked whether the direct effector-interactors exhibit evidence for balancing selection, as indicated by positive D_T values (Figure S5A). No significant deviation from random expectation could be detected for any of four effector-interactor groups: (i) all effector-interactors, (ii) interactors of effectors from two or three pathogens, (iii) interactors of effectors from three pathogens, and (iv) phenotypically supported effector-interactors (Figure S5A). For three of the four groups, the mean of D_T for effector-interactors is lower than that of random controls, whereas for the group targeted by three pathogens the mean is slightly higher.

The lack of a strong signal can likely be explained by our previous observation that many effector targets are central proteins in the network, which likely cannot tolerate much variation without adverse effects on protein function. We therefore asked whether instead there might be evidence for the selective pressure imposed by pathogens in the network neighborhood of the effector-interactors. To this end, we explored whether the AI-1_{MAIN} interaction partners of effector-interactors are subject to balancing selection, but no such evidence could be detected for any of the effector-interactor groups ($p = 0.51–0.94$) (Figure S5B). It is possible that a majority of interacting proteins mediating nonimmune functions may mask any potential signal from the few interacting proteins involved in immune functions. We therefore adopted an inverse approach and investigated whether effector-interactors are preferential interaction partners of proteins encoded by genes under balancing selection. For each cutoff of the top-ranking genes in the combined Dθ-ranked list, we counted the cumulative number of interacting effector-interactors in AI-1_{MAIN} (red dots) separately for each of the four effector groups noted above (Figure 5). To estimate the specificity of the observations in the context of the experimentally derived network structure, we performed rewiring controls of AI-1_{MAIN} and counted randomly interacting effector-interactors for the same top Dθ-ranking proteins (Figure 5A). The number of interacting effector-interactors in the real AI-1_{MAIN} network is always significantly higher than random across a range of cutoffs, demonstrating a preferential interaction of proteins

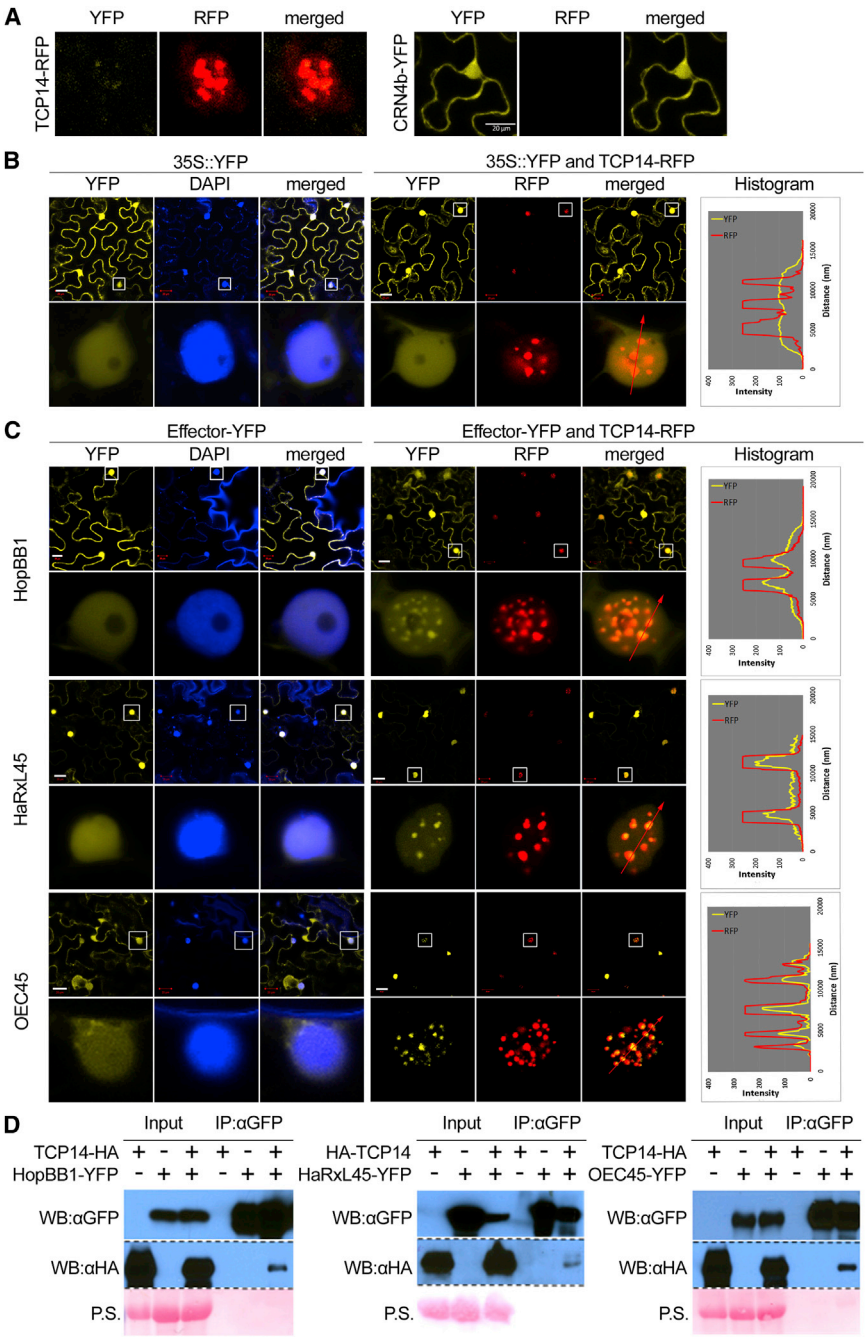

Figure 4. TCP14 Relocalizes Effectors to Subnuclear Foci

(A) Technical control demonstrating that YFP and RFP channels do not leak into each other. The images show localization of TCP14-RFP and CRN4b-YFP; image data for YFP and RFP channels were collected for both. The same settings were then applied to all assays below. Note that TCP14-YFP forms subnuclear foci.

(B and C) The lower panel exhibits an enlarged view of a representative nucleus boxed in the upper panel. The histogram illustrates the intensity of fluorescent signal across the path indicated by the red arrow. All confocal pictures were taken 40–48 hr after infiltration of Agrobacterium strains expressing the different fluorophore-tagged proteins.

(B) Negative control: TCP14 does not relocalize YFP.

(C) TCP14 relocalizes effectors from *Psy* (HopBB1), *Hpa* (HaRxL45) and *Gor* (OEC45) to subnuclear foci.

(D) TCP14 is coimmunoprecipitated by HopBB1, HaRxL45, and OEC45. All proteins were expressed from the CaMV 35S promoter in *N. benthamiana* leaves. "P.S" denotes Ponceau S staining. The 20 μM size bars ([A], right; [B] and [C] top rows) mark the first of three images from the same field. The length of a side of the nuclear images ([A], left; [B] and [C] bottom rows) is 20 μM. See also Figure S4 and Table S4.

The network of four of the top Dθ-ranking five proteins further shows that even the two interaction partners that are not effector-interactors are members of a common subnetwork by virtue of multiple interactions with variable proteins and effector-interactors (Figure 5F). The underlying biological reasons of how the increased genetic variation is beneficial in the evolutionary battle remain to be elucidated. A GO enrichment analysis of the top Dθ-ranking genes did not yield conclusive results, though, partly because many of these genes have not yet been characterized.

The evidence for preferential interaction of proteins encoded by genes under balancing selection with effector-interactors contrasts with the conservation of effector-interactors themselves, which show signs of purifying selection (Figure 5F). Together, these data demonstrate that at least a subset of proteins targeted by multiple evolutionary distant pathogens are under purifying selection, and in such instances, variation at the level of neighbors in the protein interaction network becomes a substrate for balancing selection.

encoded by genes under balancing selection with our effector-interactors. These findings are supported by similar results obtained with an AAP-based ranking, although with slightly different top-ranking proteins. These polymorphic proteins show the greatest signal with effector-interactors targeted by effectors from three pathogens. The protein with the greatest number of AAPs is an intracellular TIR-NLR type immune receptor (AT1G31540), which interacts with TCP14 and is characterized by the third-highest-ranking θ value (0.021) among all $AI\text{-}1_{MAIN}$ proteins. Previously, TIR-NLR was identified as the dominant *RAC1* gene, mediating resistance to *Albugo candida* in the Ksk-1 accession (Borhan et al., 2004).

DISCUSSION

We identified interactions between candidate virulence effector proteins from the obligate biotrophic powdery mildew fungus

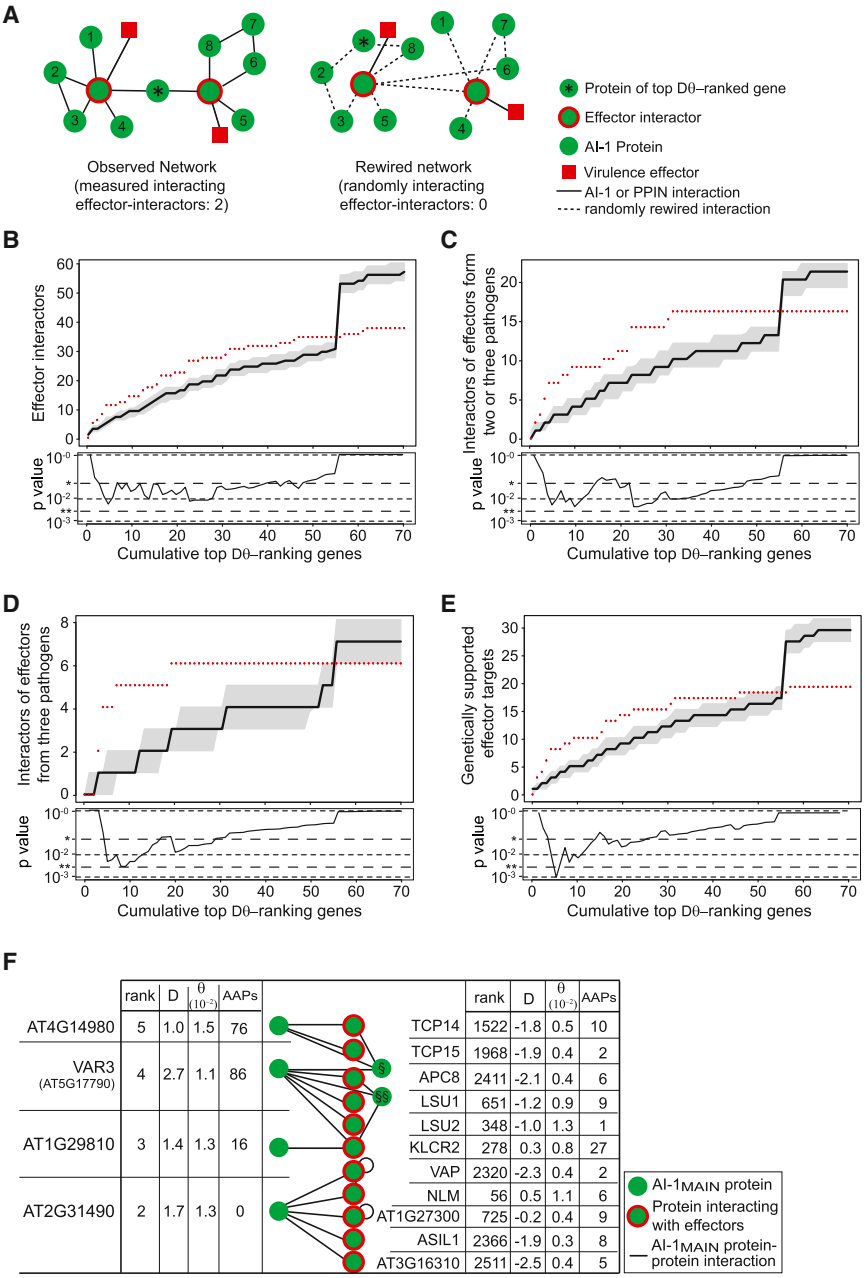

Figure 5. Proteins with High Natural Genetic Variation Interact with Effector-Interactors

(A) Schematic illustration of the analysis in (B)–(E): in the AI-1_{MAIN} network (left) the effector-interactors directly interacting with top Dθ-ranking gene products are counted and compared to the distribution of counts observed in 1,000 randomly rewired networks (single example shown). Effectors are shown for illustration only and not included in the analysis.

(B) Analysis as described in (A). Plotted along the y axis are cumulative counts of effector-interactors interacting with proteins encoded by the top Dθ-ranking x genes. Data from AI-1_{MAIN} are shown as red dots; the black line shows the median of 1,000 randomly rewired networks; gray shaded areas show the 25th and 75th percentiles of values from rewiring controls. The lower panel shows the corresponding experimental p values (* 0.05; ** 0.005). The steep rise in the simulations at x = 56 is caused by a high-degree protein (NLM1, AT4G19030) at that position; the many rewired interactions for this protein increase the count of random interactors in all categories.

(C) As in (B), but counting proteins interacting with effectors from two or three pathogens.

(D) As in (B), but counting proteins interacting with effectors from three pathogens.

(E) As in (B), but counting proteins whose mutation caused altered immune phenotypes.

(F) Among the 13 interaction partners of the five most selected proteins are eleven effector-interactors, including the five most targeted proteins. The tables show for all top Dθ-ranking proteins and effector-interactors the relative combined rank, D_T, θ_W, and the count of AAPs. The non-effector-interactor interactors of the variable proteins are § AT1G51580 and §§ ZPF7. See also Figure S5 and Table S5.

Golovinomyces orontii and proteins from its host, *Arabidopsis*. We added these to previously defined interactions between the same set of host proteins and effector suites from two pathogens derived from different kingdoms. Analysis of the combined data allowed us to significantly extend our previously defined principles of how plant pathogens have independently evolved effectors to converge onto a limited, shared set of host proteins. Our main conclusions will propel future hypothesis testing, ultimately resulting in the definition of key plant machinery modulated by diverse pathogens to increase their fitness during infection.

Our identification and analysis of *Gor* candidate effectors serves two functions. First, it paves the way for mechanistic studies of single effectors and elucidation of the infection strategies of fungal pathogens in general. Incidentally, several OECs that interact with functionally relevant targets, such as the highly connected OEC78 or the less connected OEC49 and OEC101, have homologs in *Bgh* and *Erysiphe pisi* and may be part of a putative powdery mildew core effector set (Figure 1B). Unfortunately, it was not possible to clearly differentiate host proteins as being targeted by core or noncore proteins, which prevented a deeper characterization.

Second, our systematic and unbiased identification of *Gor* effector interactors enabled combined analyses of host-pathogen interaction networks when integrated with our previous data for *Hpa* and *Psy* (Mukhtar et al., 2011). The result is a map of *Arabidopsis* proteins interacting with effectors from three destructive pathogen lineages: bacteria, oomycetes, and fungi (Figure 2A; Table S1). We demonstrate that most of the host interactors are genuine targets, in the sense that loss-of-function results in altered host immune system function (Figures 3A, 3B, and S3; Table S3). In the combined PPIN-2 network, we also significantly expand our previous evidence for interspecies effector convergence (Mukhtar et al., 2011).

We discovered evidence for combined intraspecies convergence by effectors of each of the three pathogens (Figure 2F). Our data indicate that effector-target convergence evolved independently in all kingdoms of life. Thus, convergence per se may be an important, if not necessary, feature of host-pathogen interactions. The mechanistic and evolutionary principle for this convergence is speculation, but it may suggest that successful biotrophic pathogens need to manipulate a largely shared set of physiological host networks and proteins. They may achieve this, in the face of receptor-based host immune surveillance, by homology-independent functional redundancy that uses different effectors to modulate different nodes in a common set of subnetworks, as suggested by our findings (Figure S1C). Additional pathogenicity strategies evolved by other biotrophic or nonbiotrophic pathogens may drive the evolution of idiosyncratic pathogen species-specific host targets or of completely new host machinery that is required to support lifestyles beyond those of the pathogens whose effector suites we have surveyed.

Genome sequencing of pathogenic bacterial strains revealed that effector complements are only marginally overlapping, even between strains that otherwise exhibit very high genomic sequence identity (97%) (Baltrus et al., 2011). Likewise, genome sequencing in a variety of oomycete lineages reveals diverse expansion and contraction in effector families (Pais et al., 2013; Stergiopoulos et al., 2012). Thus, the observed intraspecies convergence of effectors supports our suggestion of functional redundancy mediated by different effectors to maintain host protein targeting. The effector complement would thus be buffered against loss or rapid selection against specific effectors due to host recognition. Importantly, the plant immune system can blunt effector evolution by detecting effector-dependent host target modifications. It is much more efficient to guard a limited number of important host targets than to evolve receptors for each effector (Jones and Dangl, 2006), especially in cases where both the effector and the host receptor are under frequency-dependent balancing selection (Van der Hoorn et al., 2002). Our observations that in our systematic network (1) effectors converge onto limited number of targets and (2) a large fraction of targets, in turn, interact with highly polymorphic proteins that are under balancing selection across the *Arabidopsis* population support this notion. Alternative explanations for effector convergence include the sequential delivery of effectors targeting the same host-protein, but at different time points in the course of host colonization and/or cooperativity of effectors that might act together to modify host protein functions. Intriguingly, most *Hpa* effectors, when delivered via bacteria, conferred enhanced virulence on only a subset of *Arabidopsis* accessions in *Psy* infection assays, indicating variation between accessions in the susceptibility to effector manipulation (Fabro et al., 2011).

Integrating these network concepts with our extensive reverse genetic data, we demonstrate that effector convergences strongly correlate with mutant infection phenotypes (Figures 3B–3E). Our genetic data convincingly reinforce our interpretation that network convergence is due to selection of effector interactions with host proteins. Our mutant phenotyping results also show that most host targets of multiple pathogens have previously unknown plant immune system functions. This conclusion is substantiated by the fact that effector-interactors are also preferential interaction partners of intracellular NLR receptors, likely reflecting guarding of these virulence targets by the plant immune system (Mukhtar et al., 2011).

To demonstrate that interactions between effectors and highly targeted host-proteins can occur in planta, we investigated TCP14, the host protein most commonly targeted by effectors. These experiments demonstrated that the majority of tested effectors that interact with TCP14 in Y2H are relocalized in the nucleus to characteristic TCP14 subnuclear foci (Figure 4C and S4; Table S4). The function of the TCP14 foci and the function(s) of specific effectors within them are now the object of active investigation. Together with extended genetic support for TCP14 function in response to infection, our findings strengthen the hypothesis that the majority of effector-TCP14 interactions reflect genuine protein-protein interactions that function during infections by diverse pathogens.

Plants and microbial pathogens are engaged in a constant evolutionary battle in which pathogens can expand their suites of effectors via horizontal gene transfer, or evolution of new alleles of existing effectors, driving selection in plants to respond accordingly. Each successful evolutionary step in the plant can be overcome by subsequent modification of pathogen effector deployment. Yet both pathogen virulence and plant immune function have fitness costs that can drive the arms race into balanced trench warfare (Holub, 2001). The current shape of the plant immune system is a consequence of these counteracting forces. The network we define here is uniquely well supported by broad mutant phenotype analysis and cell biological investigation.

EXPERIMENTAL PROCEDURES

Effector Prediction and Cloning

Secreted proteins were identified in a cDNA library from isolated haustoria by employing SignalP3.0 at a HMM threshold of 0.8 and the TMHMM algorithm (http://www.cbs.dtu.dk/services/TMHMM) (Bendtsen et al., 2004). A size cut-off of $\geq$60 amino acids was applied. The absence of homologs in unrelated species was confirmed by BLAST. In a second prediction round, 491 *Bgh* Candidates for Secreted Effector Proteins (Pedersen et al., 2012) and effector candidates from the first round were used as templates for tBLASTn and BLASTp analyses of the haustorial cDNA library. Putative homologs of predicted effectors were then subjected to SignalP3.0 and TMHMM analysis, and the absence of homologs in unrelated species was confirmed to prevent false positives. Finally, the conservation of OECs in the genomes of *Bgh* and *E. pisi* was queried by tBLASTn. A multiple sequence alignment of the *OECs* was generated using ClustalW (http://www.ebi.ac.uk/Tools/msa/clustalw2/) and imported into MEGA5 (Tamura et al., 2011). The phylogeny was computed with default parameters using the Neighbor-joining algorithm and a p-distance model for amino acid substitutions. For *OEC* cloning, primers spanning the mature protein (without signal peptide) were generated and used for PCR from a mix of cDNA constructed from plant material at 1, 3, 5, and 10 dpi with *G. orontii* using a proof-reading polymerase.

Y2H Analysis

A detailed description of the Y2H pipeline can be found in the Supplemental Information.

Phenotypic Assays

We used *Arabidopsis thaliana* Columbia (Col-0) unless mentioned otherwise. Single mutants for *eds1-2* (Bartsch et al., 2006), *sid2-2* (Dewdney et al., 2000), and *mlo2-6* (Consonni et al., 2006) in the Col-0 genetic background were used as controls for the relevant infection assays. The set of homozygous T-DNA insertion lines is described in Table S3. Pathogen infection assays were performed as described in the Supplemental Experimental Procedures.

Statistical Analysis

Details of the statistical analyses and controls can be found in the Supplemental Information.

Relocalization of Effectors by TCP14

Vector constructs: Coding sequences of *Psy* effectors and coding sequences of *Hpa* and *Gor* effectors lacking the signal peptides were amplified by PCR and then Gateway-cloned into the destination vectors pGWB41, pGWB660, pGWB642, pGWB644, pGWB645, and a modified pMDC7, respectively (Akimoto-Tomiyama et al., 2012; Nakagawa et al., 2007) (Table S4). The plasmids were transformed into the *Agrobacterium tumefaciens* strain GV3101 for transient expression assays in *Nicotiana benthamiana* (see Supplemental Experimental Procedures).

Immunoprecipitation

HA-tagged TCP14 and eYFP-tagged effectors were expressed in *N. benthamiana* under control of the 35S constitutive promoter. The binary vectors used for expression were pGWB614 (for TCP14-HA), pGWB715 (for HA-TCP14), pGWB641 (for HaRxL45-YFP and HopBB1-YFP), and pGWB41 (for OEC45-YFP). Agrobacteria carrying each construct (OD = 0.2) were infiltrated into *N. benthamiana* leaves 24 hr prior to harvesting. Proteins were extracted from 0.5 g of fresh tissue using 2 ml extraction buffer (50 mM HEPES [pH 7.5], 50 mM NaCl, 10 mM EDTA [pH 8.0], 0.5% Triton X-100, 5 mM DTT, and 1x Plant protease inhibitor cocktail from Sigma-Aldrich). Magnetic labeling and separation of tagged proteins was performed using μMACS Epitope Tag Protein Isolation Kit (Miltenyi Biotec). Protein samples were separated by 12% SDS-PAGE. Immunoblots were performed with a 1:1,000 dilution of α-HA (Roche) and 1:1,000 dilution of α-GFP (Roche). Blots were detected by ECL prime (GE Healthcare).

ACCESSION NUMBERS

The GenBank accession numbers for the *G. orontii* effector candidate (*OEC*) sequences reported in this paper are KM220803–KM220886.

All GenBank accession numbers are further listed and associated with the correct OECs in Table S1.

SUPPLEMENTAL INFORMATION

Supplemental Information includes five figures, five tables, and Supplemental Experimental Procedures and can be found with this article online at http://dx.doi.org/10.1016/j.chom.2014.08.004.

AUTHOR CONTRIBUTIONS

OEC identification and cloning: R.W., A.E.S., E.V.L.v.T., and R.P. OEC-At interactome mapping: R.W., L.G., J.R.E., M.V., and P.B. Data integration and convergence statistics: S.A., C.G., K.F.X.M., J.L.D., and P.B. Immune assays (*Hpa*, *Psy*): P.E., K.W., N.M., M.S.M., and J.L.D. Immune assays (*Gor*): R.W., S.H., P.S.-L., and R.P. Phenotype statistics: S.A., P.E., R.W., E.V.L.v.T., and P.B. Colocalization analysis: Y.H., L.Y., and J.L.D. Immunoprecipitations: L.Y., Y.H., and J.L.D. Provision of several *Hpa* effectors: J.D.G.J.; natural variation analysis: S.A., S.R.H., K.C.B., K.F.X.M., D.W., J.L.D., and P.B. Manuscript writing: P.B., P.E., S.A., R.W., and J.L.D. Critical manuscript reading and editing: P.S.-L. and R.P. Conception and design: P.E., R.P., P.B., and J.L.D.

ACKNOWLEDGMENTS

We thank Axel Künstner for helpful discussions about the population genetic analysis. This work was funded by grants to J.L.D. from the National Science Foundation (IOS-1257373), the National Institutes of Health (1RO1 GM107444), the Gordon and Betty Moore Foundation (GBMF3030), and the HHMI. R.W. was supported by a PhD fellowship from the International Max-Planck Research School (IMPRS). J.L.D. is an Investigator of the Howard Hughes Medical Institute. L.Y. was funded in part by the Gordon and Betty Moore Foundation through Grant GBMF 2550.02 to the Life Sciences Research Foundation. Y.H. was supported by a Distinguished Guest Professorship, Eberhard-Karls-Universität, Tübingen, Germany to J.L.D. S.A. and P.B. are supported by the Deutsche Forschungsgemeinschaft (DFG) grant SFB924. R.P. and P.S.-L. were supported by grants from the Max-Planck society. We thank Dr. Meng Chen, Duke University, for 35S:phyB-CFP and useful discussions regarding subnuclear foci.

Received: March 23, 2014
Revised: June 27, 2014
Accepted: August 14, 2014
Published: September 10, 2014

REFERENCES

Akimoto-Tomiyama, C., Furutani, A., Tsuge, S., Washington, E.J., Nishizawa, Y., Minami, E., and Ochiai, H. (2012). XopR, a type III effector secreted by *Xanthomonas oryzae* pv. oryzae, suppresses microbe-associated molecular pattern-triggered immunity in *Arabidopsis thaliana*. Mol. Plant Microbe Interact. *25*, 505–514.

Alonso, J.M., and Ecker, J.R. (2006). Moving forward in reverse: genetic technologies to enable genome-wide phenomic screens in *Arabidopsis*. Nat. Rev. Genet. *7*, 524–536.

Baltrus, D.A., Nishimura, M.T., Romanchuk, A., Chang, J.H., Mukhtar, M.S., Cherkis, K., Roach, J., Grant, S.R., Jones, C.D., and Dangl, J.L. (2011). Dynamic evolution of pathogenicity revealed by sequencing and comparative genomics of 19 *Pseudomonas syrinage* isolates. PLoS Pathog. *7*, e1002132.

Bartsch, M., Gobbato, E., Bednarek, P., Debey, S., Schultze, J.L., Bautor, J., and Parker, J.E. (2006). Salicylic acid-independent ENHANCED DISEASE SUSCEPTIBILITY1 signaling in *Arabidopsis* immunity and cell death is regulated by the monooxygenase *FMO1* and the Nudix hydrolase *NUDT7*. Plant Cell *18*, 1038–1051.

Baxter, L., Tripathy, S., Ishaque, N., Boot, N., Cabral, A., Kemen, E., Thines, M., Ah-Fong, A., Anderson, R., Badejoko, W., et al. (2010). Signatures of adaptation to obligate biotrophy in the *Hyaloperonospora arabidopsidis* genome. Science *330*, 1549–1551.

Bendtsen, J.D., Nielsen, H., von Heijne, G., and Brunak, S. (2004). Improved prediction of signal peptides: SignalP 3.0. J. Mol. Biol. *340*, 783–795.

Borhan, M.H., Holub, E.B., Beynon, J.L., Rozwadowski, K., and Rimmer, S.R. (2004). The *Arabidopsis* TIR-NB-LRR gene *RAC1* confers resistance to *Albugo candida* (white rust) and is dependent on *EDS1* but not *PAD4*. Mol. Plant Microbe Interact. *17*, 711–719.

Braun, P. (2012). Interactome mapping for analysis of complex phenotypes: insights from benchmarking binary interaction assays. Proteomics *12*, 1499–1518.

Caillaud, M.C., Piquerez, S.J., Fabro, G., Steinbrenner, J., Ishaque, N., Beynon, J., and Jones, J.D. (2012). Subcellular localization of the *Hpa* RxLR effector repertoire identifies a tonoplast-associated protein HaRxL17 that confers enhanced plant susceptibility. Plant J. *69*, 252–265.

Cao, J., Schneeberger, K., Ossowski, S., Günther, T., Bender, S., Fitz, J., Koenig, D., Lanz, C., Stegle, O., Lippert, C., et al. (2011). Whole-genome sequencing of multiple *Arabidopsis thaliana* populations. Nat. Genet. *43*, 956–963.

Chen, M., Tao, Y., Lim, J., Shaw, A., and Chory, J. (2005). Regulation of phytochrome B nuclear localization through light-dependent unmasking of nuclear-localization signals. Curr. Biol. *15*, 637–642.

Chisholm, S.T., Coaker, G., Day, B., and Staskawicz, B.J. (2006). Host-microbe interactions: shaping the evolution of the plant immune response. Cell *124*, 803–814.

Consonni, C., Humphry, M.E., Hartmann, H.A., Livaja, M., Durner, J., Westphal, L., Vogel, J., Lipka, V., Kemmerling, B., Schulze-Lefert, P., et al. (2006). Conserved requirement for a plant host cell protein in powdery mildew pathogenesis. Nat. Genet. *38*, 716–720.

Consortium, A.I.M.; Arabidopsis Interactome Mapping Consortium (2011). Evidence for network evolution in an *Arabidopsis* interactome map. Science *333*, 601–607.

Dangl, J.L., Horvath, D.M., and Staskawicz, B.J. (2013). Pivoting the plant immune system from dissection to deployment. Science *341*, 746–751.

Deslandes, L., and Rivas, S. (2012). Catch me if you can: bacterial effectors and plant targets. Trends Plant Sci. *17*, 644–655.

Dewdney, J., Reuber, T.L., Wildermuth, M.C., Devoto, A., Cui, J., Stutius, L.M., Drummond, E.P., and Ausubel, F.M. (2000). Three unique mutants of *Arabidopsis* identify *eds* loci required for limiting growth of a biotrophic fungal pathogen. Plant J. *24*, 205–218.

Dodds, P.N., and Rathjen, J.P. (2010). Plant immunity: towards an integrated view of plant-pathogen interactions. Nat. Rev. Genet. *11*, 539–548.

Dreze, M., Monachello, D., Lurin, C., Cusick, M.E., Hill, D.E., Vidal, M., and Braun, P. (2010). High-quality binary interactome mapping. Methods Enzymol. *470*, 281–315.

Fabro, G., Steinbrenner, J., Coates, M., Ishaque, N., Baxter, L., Studholme, D.J., Körner, E., Allen, R.L., Piquerez, S.J., Rougon-Cardoso, A., et al. (2011). Multiple candidate effectors from the oomycete pathogen *Hyaloperonospora arabidopsidis* suppress host plant immunity. PLoS Pathog. *7*, e1002348.

Feng, F., and Zhou, J.M. (2012). Plant-bacterial pathogen interactions mediated by type III effectors. Curr. Opin. Plant Biol. *15*, 469–476.

Hacquard, S., Kracher, B., Maekawa, T., Vernaldi, S., Schulze-Lefert, P., and Ver Loren van Themaat, E. (2013). Mosaic genome structure of the barley powdery mildew pathogen and conservation of transcriptional programs in divergent hosts. Proc. Natl. Acad. Sci. USA *110*, E2219–E2228.

Holub, E.B. (2001). The arms race is ancient history in *Arabidopsis*, the wildflower. Nat. Rev. Genet. *2*, 516–527.

Jones, J.D., and Dangl, J.L. (2006). The plant immune system. Nature *444*, 323–329.

Kemen, E., and Jones, J.D.G. (2012). Obligate biotroph parasitism: can we link genomes to lifestyles? Trends Plant Sci. *17*, 448–457.

Kim, S.H., Son, G.H., Bhattacharjee, S., Kim, H.J., Nam, J.C., Nguyen, P.D., Hong, J.C., and Gassmann, W. (2014). The Arabidopsis immune adaptor SRFR1 interacts with TCP transcription factors that redundantly contribute to effector-triggered immunity. Plant J. *78*, 978–989.

Markow, A.V. (2005). On the origin of the eukaryotic cell. Paleontol. J. *39*, 109–116.

Martín-Trillo, M., and Cubas, P. (2010). TCP genes: a family snapshot ten years later. Trends Plant Sci. *15*, 31–39.

Micali, C., Göllner, K., Humphry, M., Consonni, C., and Panstruga, R. (2008). The powdery mildew disease of Arabidopsis: A paradigm for the interaction between plants and biotrophic fungi. Arabidopsis Book *6*, e0115.

Mukhtar, M.S., Carvunis, A.-R., Dreze, M., Epple, P., Steinbrenner, J., Moore, J., Tasan, M., Galli, M., Hao, T., Nishimura, M.T., et al.; European Union Effectoromics Consortium (2011). Independently evolved virulence effectors converge onto hubs in a plant immune system network. Science *333*, 596–601.

Nakagawa, T., Kurose, T., Hino, T., Tanaka, K., Kawamukai, M., Niwa, Y., Toyooka, K., Matsuoka, K., Jinbo, T., and Kimura, T. (2007). Development of series of gateway binary vectors, pGWBs, for realizing efficient construction of fusion genes for plant transformation. J. Biosci. Bioeng. *104*, 34–41.

Pais, M., Win, J., Yoshida, K., Etherington, G.J., Cano, L.M., Raffaele, S., Banfield, M.J., Jones, A., Kamoun, S., and Go Saunders, D. (2013). From pathogen genomes to host plant processes: the power of plant parasitic oomycetes. Genome Biol. *14*, 211.

Pardey, P.G., Beddow, J.M., Kriticos, D.J., Hurley, T.M., Park, R.F., Duveiller, E., Sutherst, R.W., Burdon, J.J., and Hodson, D. (2013). Agriculture. Right-sizing stem-rust research. Science *340*, 147–148.

Pedersen, C., Ver Loren van Themaat, E., McGuffin, L.J., Abbott, J.C., Burgis, T.A., Barton, G., Bindschedler, L.V., Lu, X., Maekawa, T., Wessling, R., et al. (2012). Structure and evolution of barley powdery mildew effector candidates. BMC Genomics *13*, 694.

Pieterse, C.M., Van der Does, D., Zamioudis, C., Leon-Reyes, A., and Van Wees, S.C. (2012). Hormonal modulation of plant immunity. Annu. Rev. Cell Dev. Biol. *28*, 489–521.

Raffaele, S., and Kamoun, S. (2012). Genome evolution in filamentous plant pathogens: why bigger can be better. Nat. Rev. Microbiol. *10*, 417–430.

Robert-Seilaniantz, A., Grant, M., and Jones, J.D. (2011). Hormone crosstalk in plant disease and defense: more than just jasmonate-salicylate antagonism. Annu. Rev. Phytopathol. *49*, 317–343.

Spanu, P.D., Abbott, J.C., Amselem, J., Burgis, T.A., Soanes, D.M., Stüber, K., Ver Loren van Themaat, E., Brown, J.K.M., et al. (2010). Genome expansion and gene loss in powdery mildew fungi reveal functional tradeoffs in parasitism. Science *330*, 1543–1546.

Stergiopoulos, I., Kourmpetis, Y.A., Slot, J.C., Bakker, F.T., De Wit, P.J., and Rokas, A. (2012). In silico characterization and molecular evolutionary analysis of a novel superfamily of fungal effector proteins. Mol. Biol. Evol. *29*, 3371–3384.

Sugio, A., Kingdom, H.N., MacLean, A.M., Grieve, V.M., and Hogenhout, S.A. (2011). Phytoplasma protein effector SAP11 enhances insect vector reproduction by manipulating plant development and defense hormone biosynthesis. Proc. Natl. Acad. Sci. USA *108*, E1254–E1263.

Tajima, F. (1989). Statistical method for testing the neutral mutation hypothesis by DNA polymorphism. Genetics *123*, 585–595.

Tamura, K., Peterson, D., Peterson, N., Stecher, G., Nei, M., and Kumar, S. (2011). MEGA5: molecular evolutionary genetics analysis using maximum likelihood, evolutionary distance, and maximum parsimony methods. Mol. Biol. Evol. *28*, 2731–2739.

van der Biezen, E.A., Freddie, C.T., Kahn, K., Parker, J.E., and Jones, J.D. (2002). *Arabidopsis RPP4* is a member of the *RPP5* multigene family of TIR-NB-LRR genes and confers downy mildew resistance through multiple signalling components. Plant J. *29*, 439–451.

Van der Hoorn, R.A., De Wit, P.J., and Joosten, M.H. (2002). Balancing selection favors guarding resistance proteins. Trends Plant Sci. *7*, 67–71.

Watterson, G.A. (1975). On the number of segregating sites in genetical models without recombination. Theor. Popul. Biol. *7*, 256–276.

Weßling, R., Schmidt, S.M., Micali, C.O., Knaust, F., Reinhardt, R., Neumann, U., Ver Loren van Themaat, E., and Panstruga, R. (2012). Transcriptome analysis of enriched *Golovinomyces orontii* haustoria by deep 454 pyrosequencing. Fungal Genet. Biol. *49*, 470–482.

Wicker, T., Oberhaensli, S., Parlange, F., Buchmann, J.P., Shatalina, M., Roffler, S., Ben-David, R., Doležel, J., Šimková, H., Schulze-Lefert, P., et al. (2013). The wheat powdery mildew genome shows the unique evolution of an obligate biotroph. Nat. Genet. *45*, 1092–1096.

Win, J., Chaparro-Garcia, A., Belhaj, K., Saunders, D.G., Yoshida, K., Dong, S., Schornack, S., Zipfel, C., Robatzek, S., Hogenhout, S.A., and Kamoun, S. (2012). Effector biology of plant-associated organisms: concepts and perspectives. Cold Spring Harb. Symp. Quant. Biol. *77*, 235–247.

Cell Host & Microbe, Volume *16*

Supplemental Information

Convergent Targeting of a Common Host

Protein-Network by Pathogen

Effectors from Three Kingdoms of Life

Ralf Weßling, Petra Epple, Stefan Altmann, Yijian He, Li Yang, Stefan R. Henz, Nathan McDonald, Kristin Wiley, Kai Christian Bader, Christine Gläßer, M. Shahid Mukhtar, Sabine Haigis, Lila Ghamsari, Amber E. Stephens, Joseph R. Ecker, Marc Vidal, Jonathan D.G. Jones, Klaus F.X. Mayer, Emiel Ver Loren van Themaat, Detlef Weigel, Paul Schulze-Lefert, Jeffery L. Dangl, Ralph Panstruga, and Pascal Braun

Figure S1, related to Figure 1

A

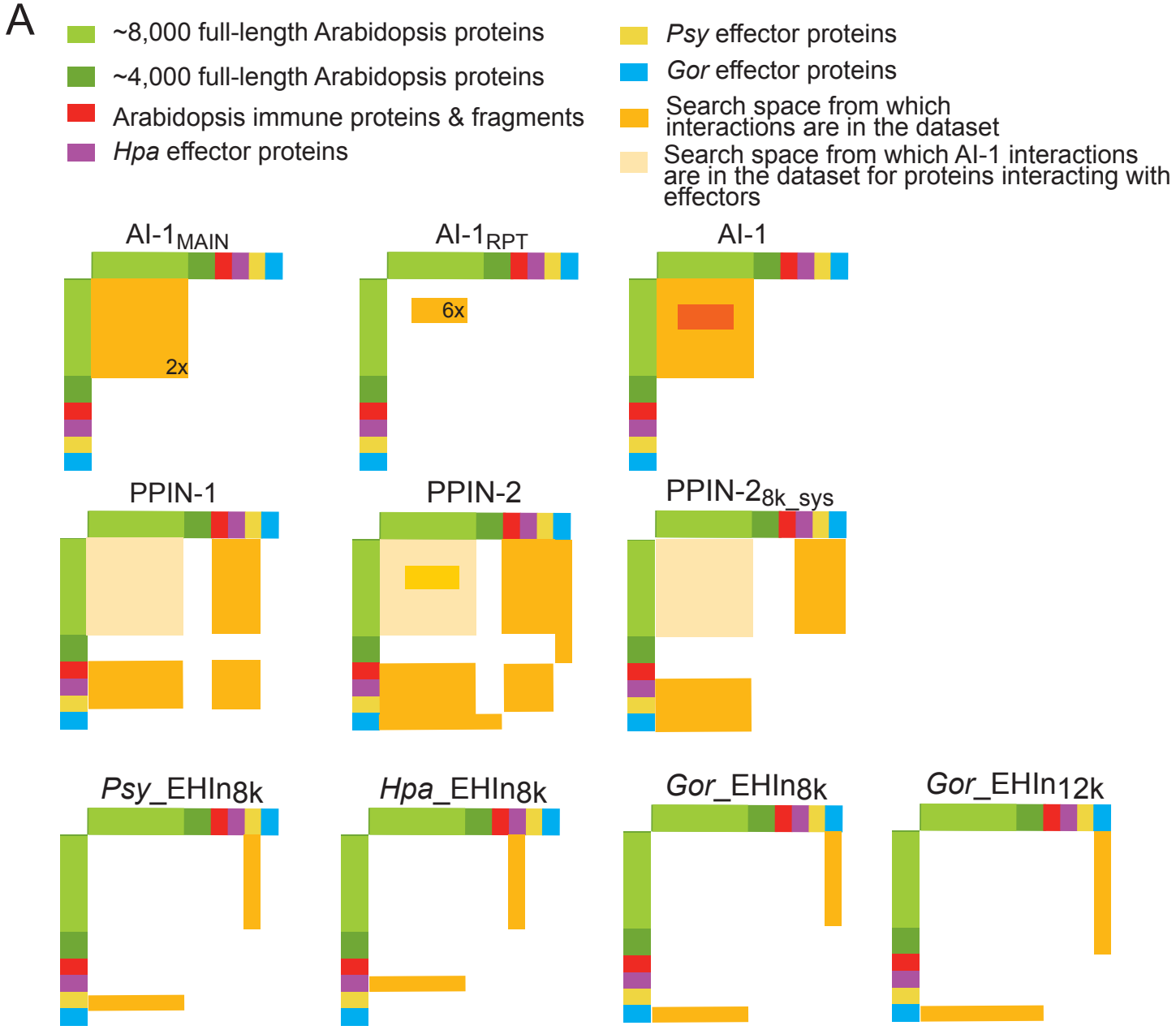

B

		Psy	*Hpa*	*Gor*	nr_Sum
8k Space	Effectors_8k	30	52	41	123
	Host-Interactors_8k	56	118	45	178
	Host-Interactors$_{AI\text{-}1MAIN}$	47	107	42	155
	Effector-host protein Interactions_8k	99	230	93	422
12k Space	Effectors_12k	-	-	46	46
	Interactors_12k	-	-	60	60
	Effector-Host-protein Interactions_12k	-	-	122	122
PPIN-1	Effectors	30	53	-	83
	Interactors_8K+Imm	61	122	-	165
	Effector-host-protein Interactions_8k+Imm	106	234	-	340

Figure 1C, related to Figure 1

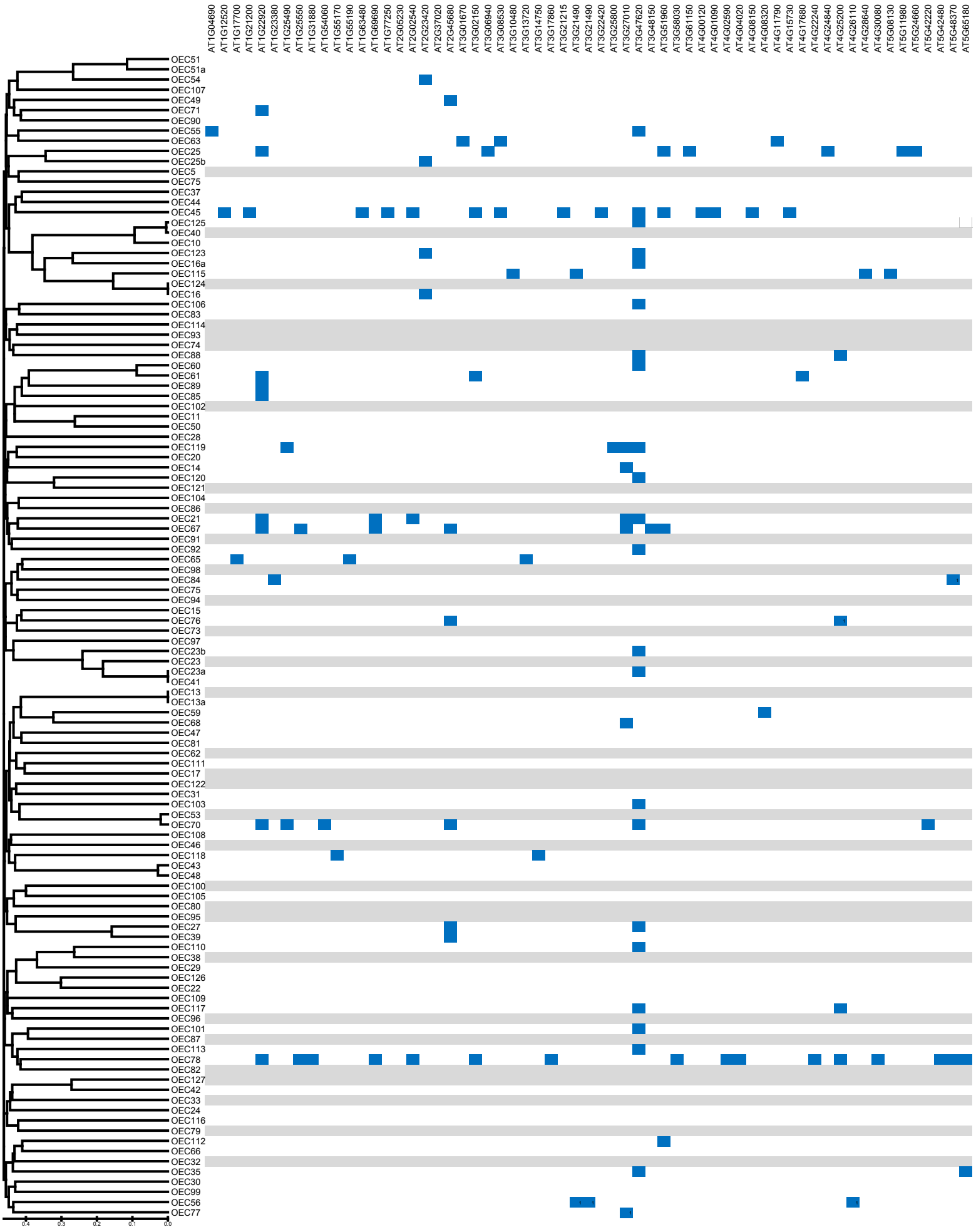

Figure S2, related to Figure 2

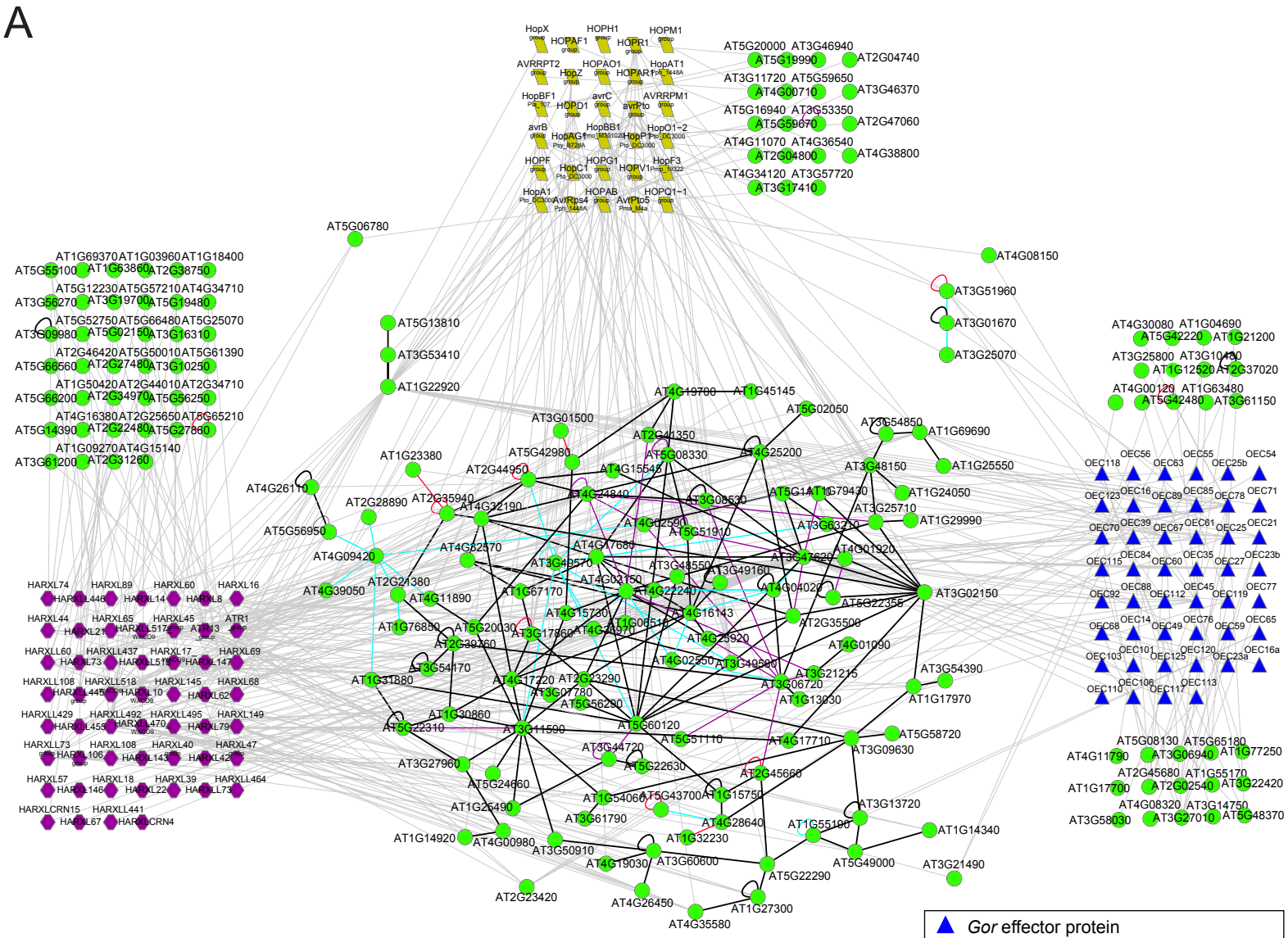

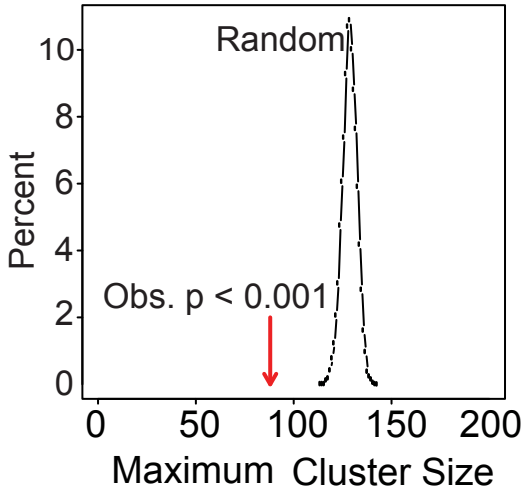

Figure S3, related to Figure 3

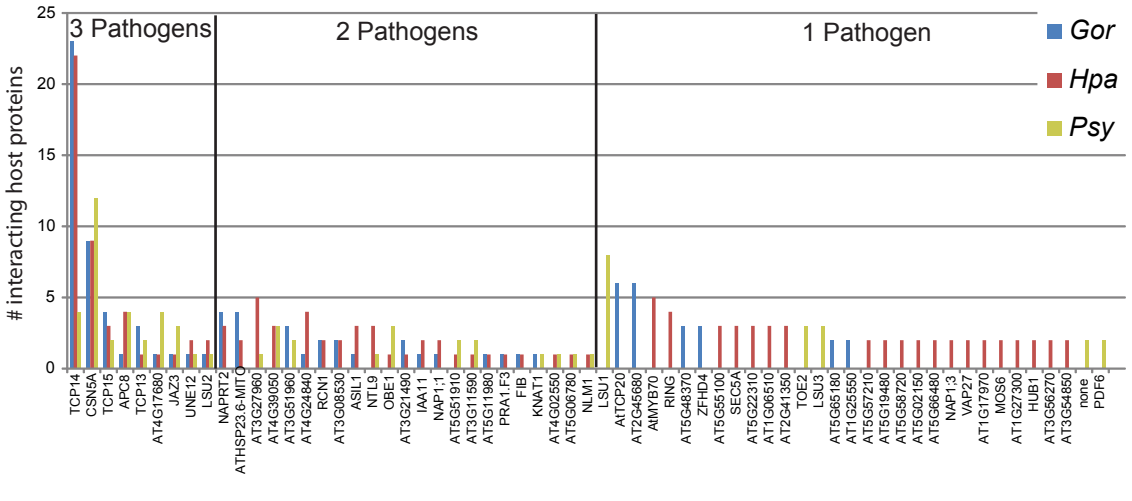

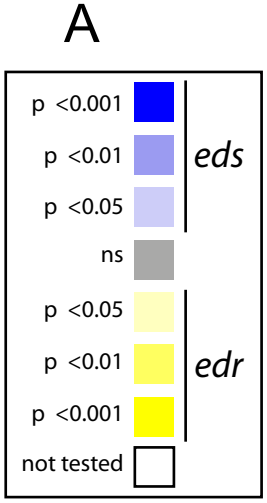

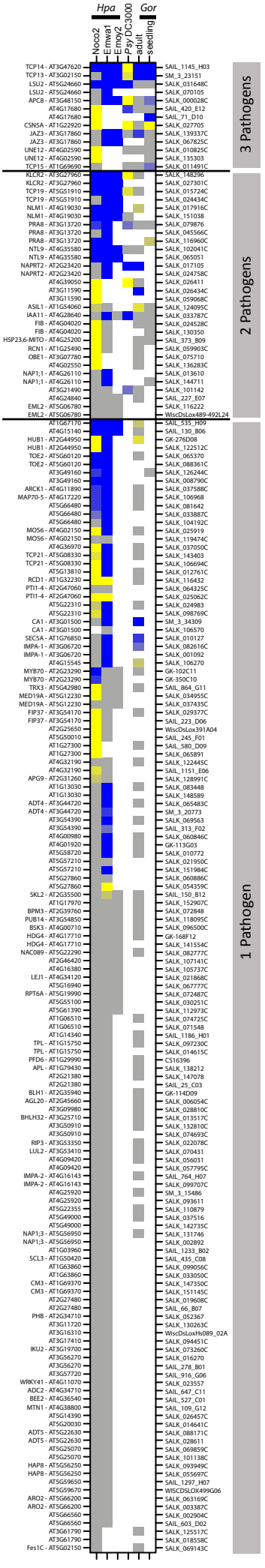

Figure S4, related to Figure 4

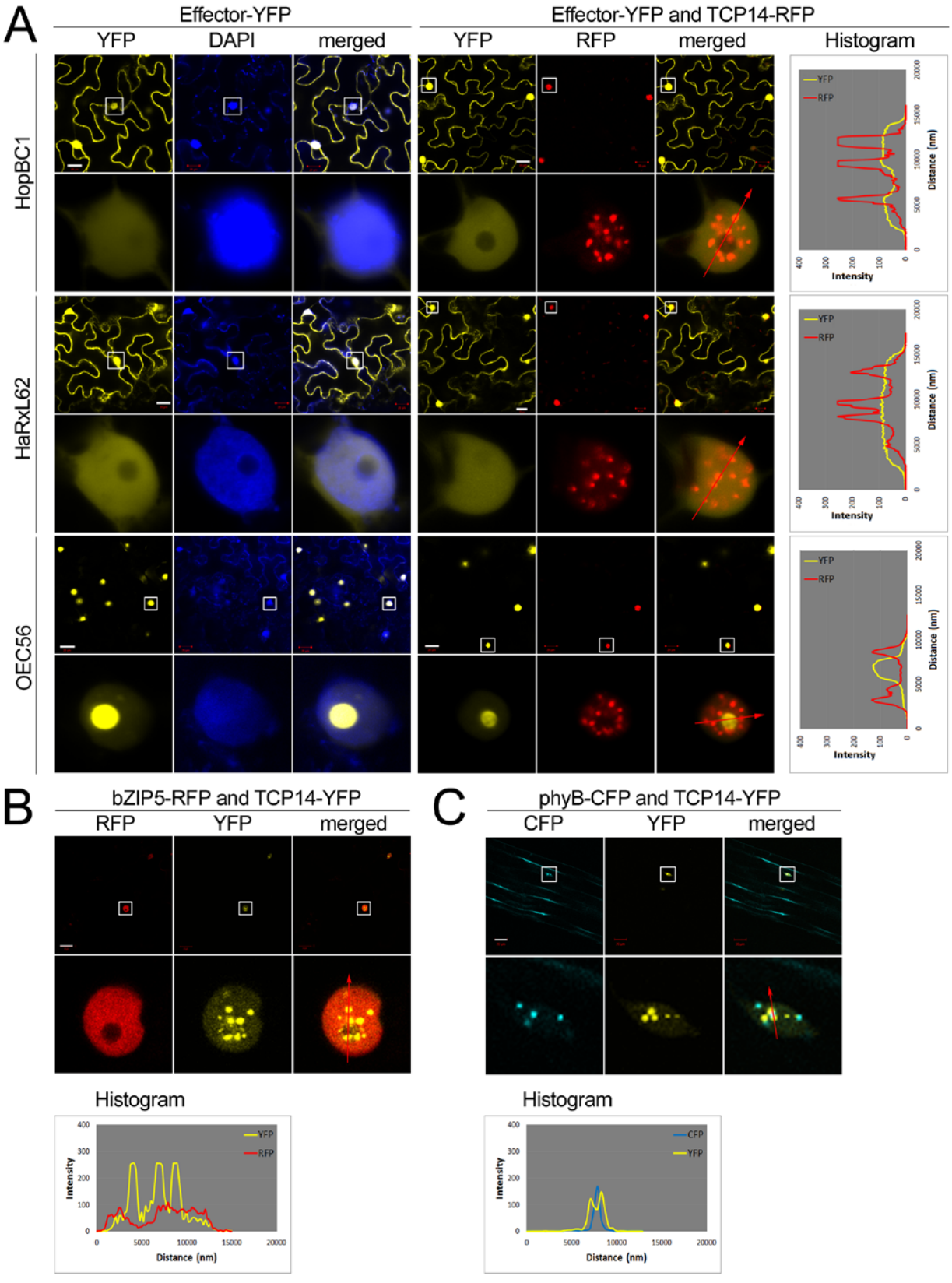

Figure S4, related to Figure 4

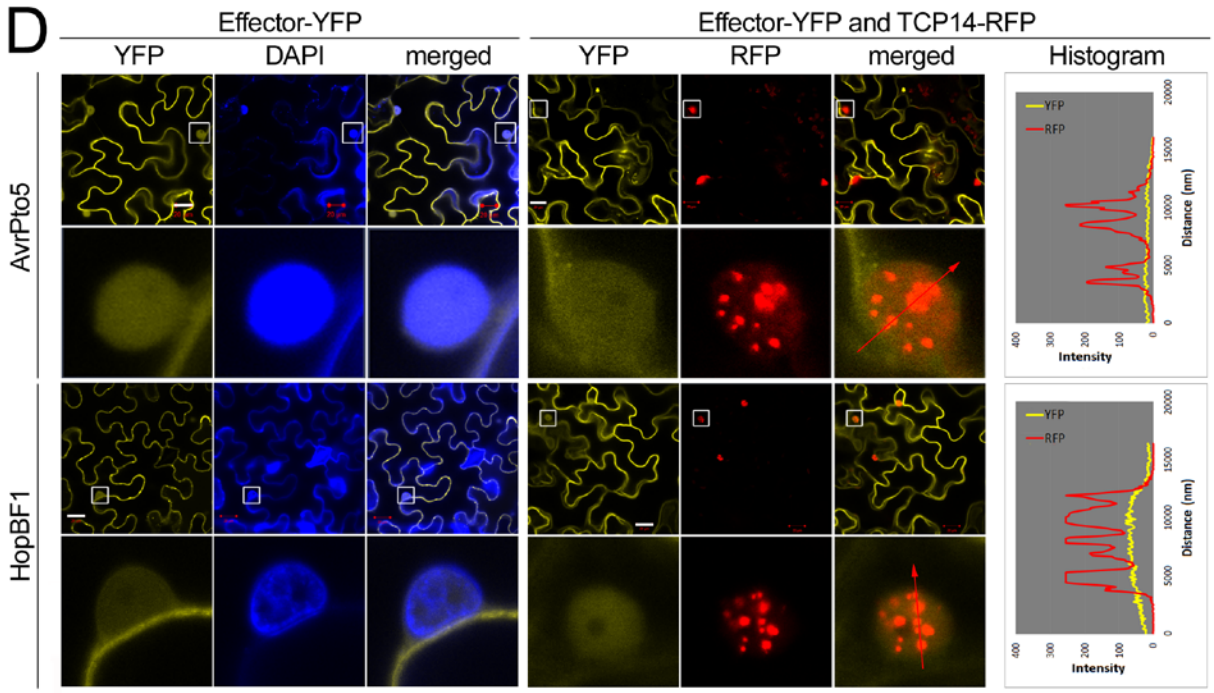

Figure S4, related to Figure 4

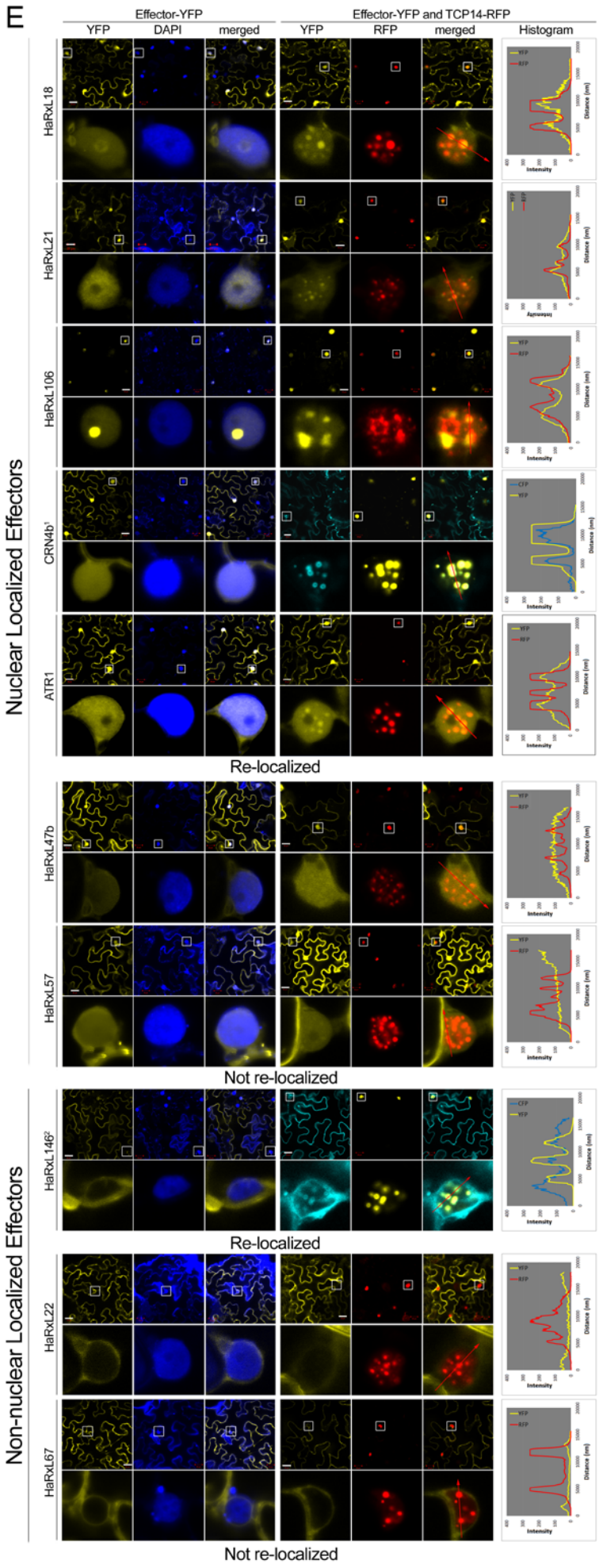

Figure S4, related to Figure 4

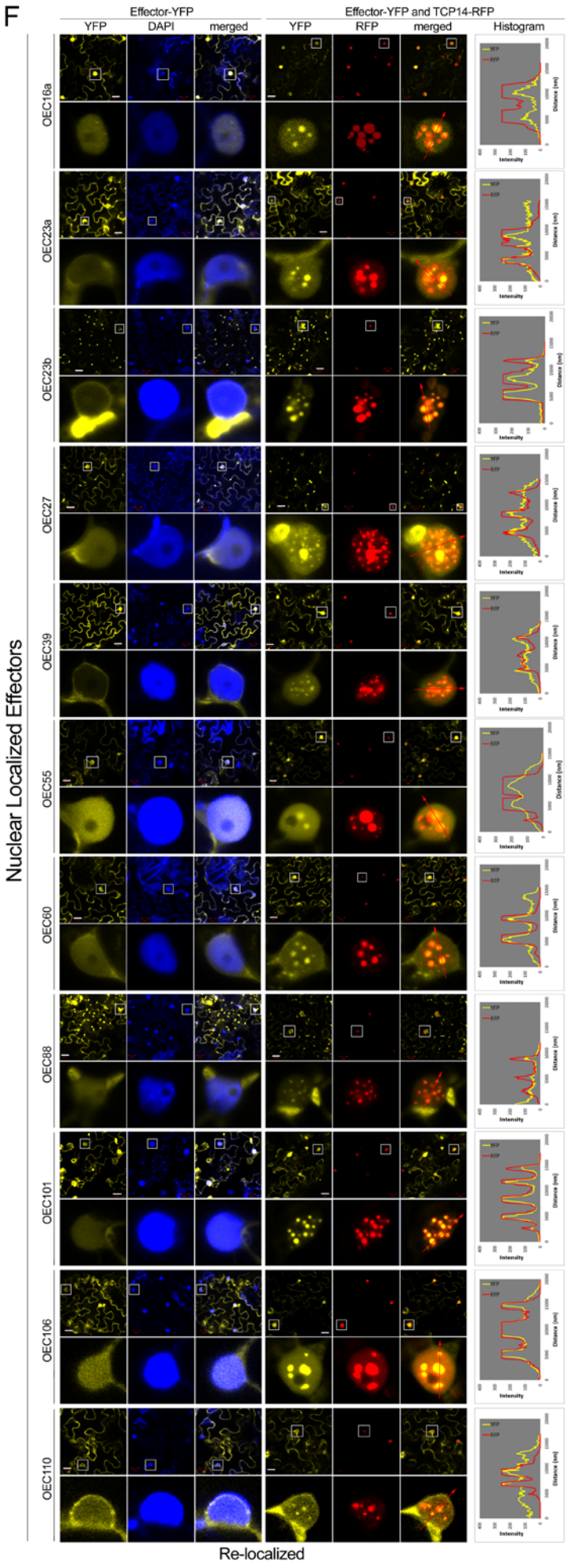

Figure S4, related to Figure 4

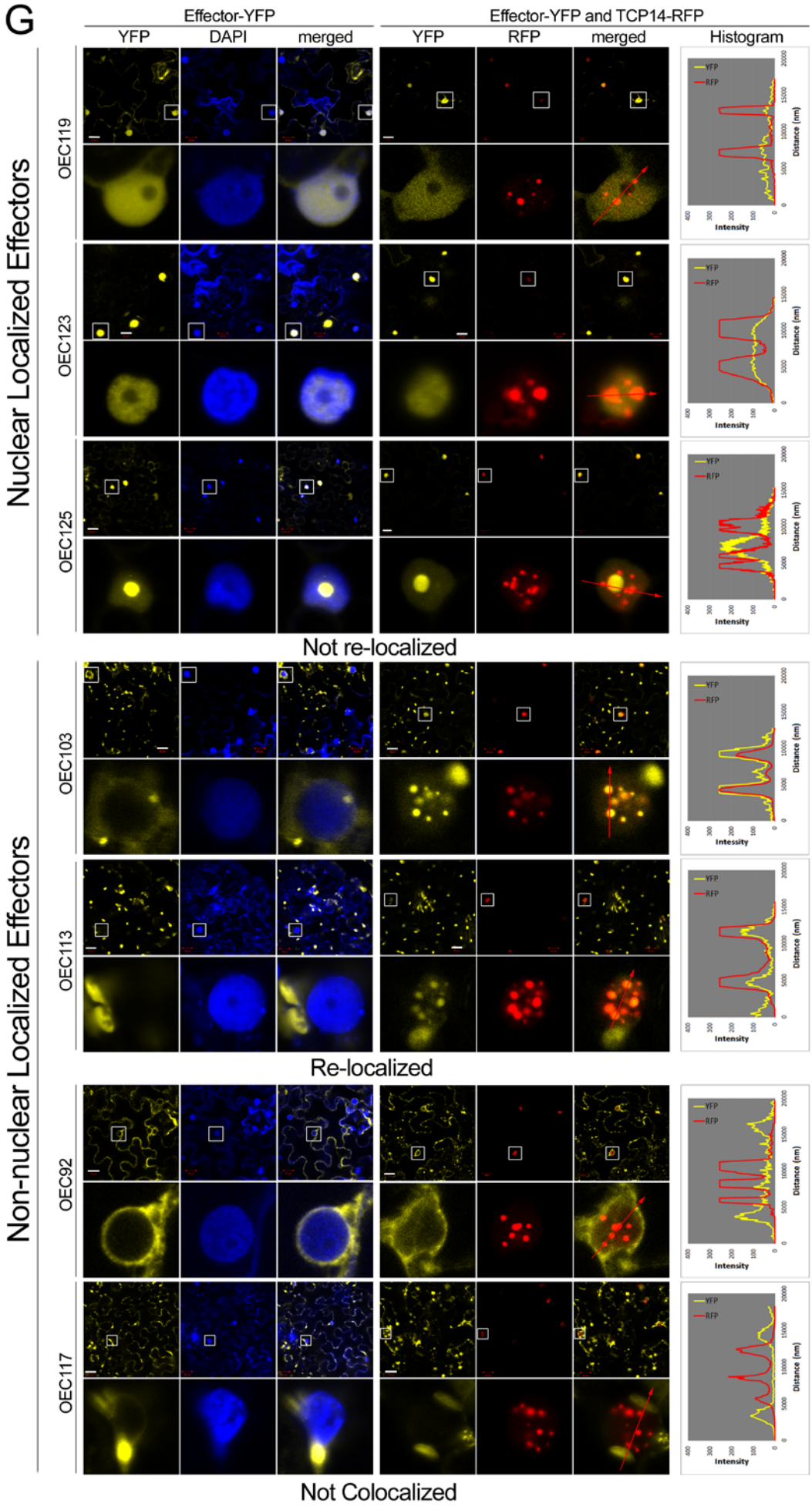

Figure S4, related to Figure 4

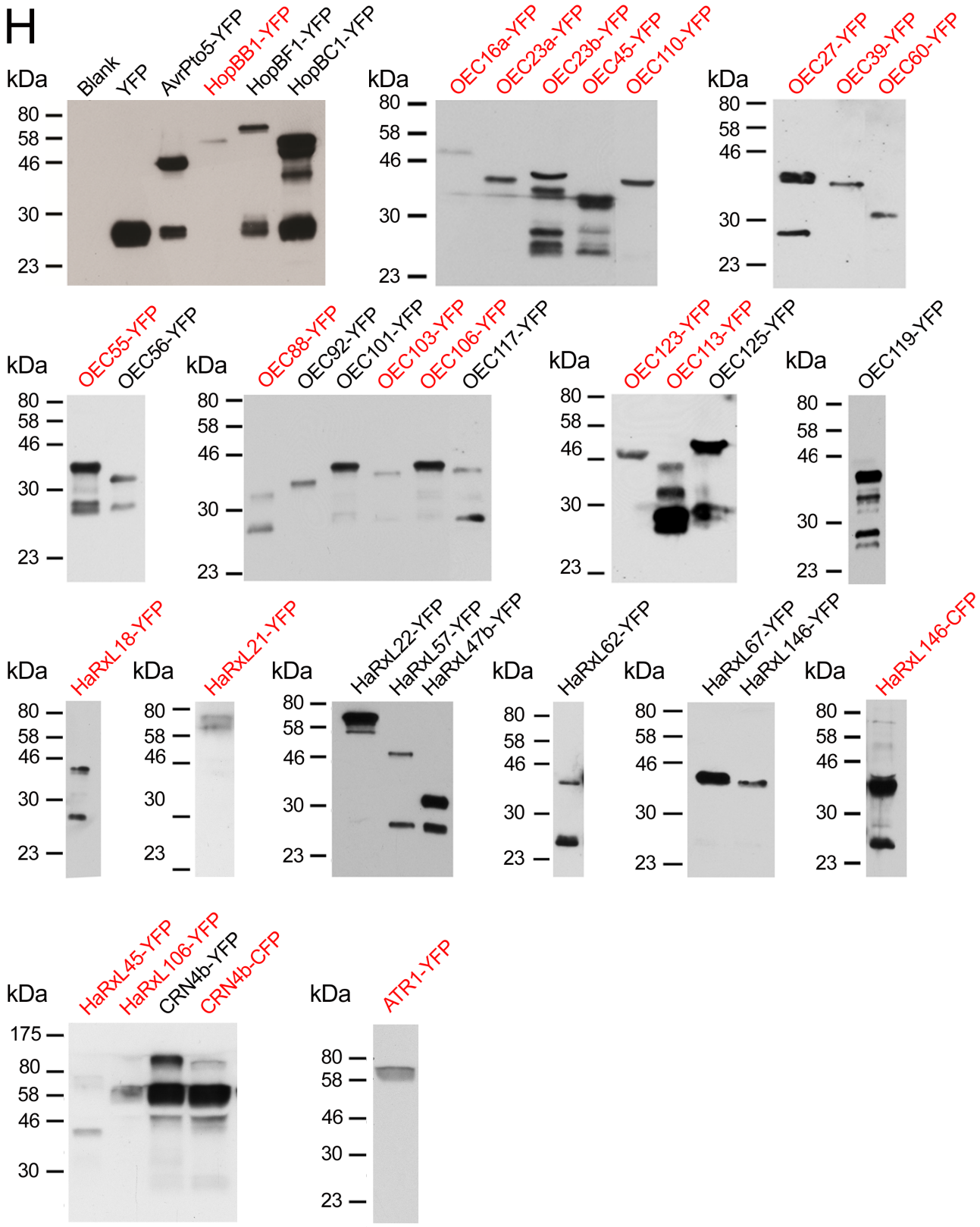

Figure S5, related to Figure 5

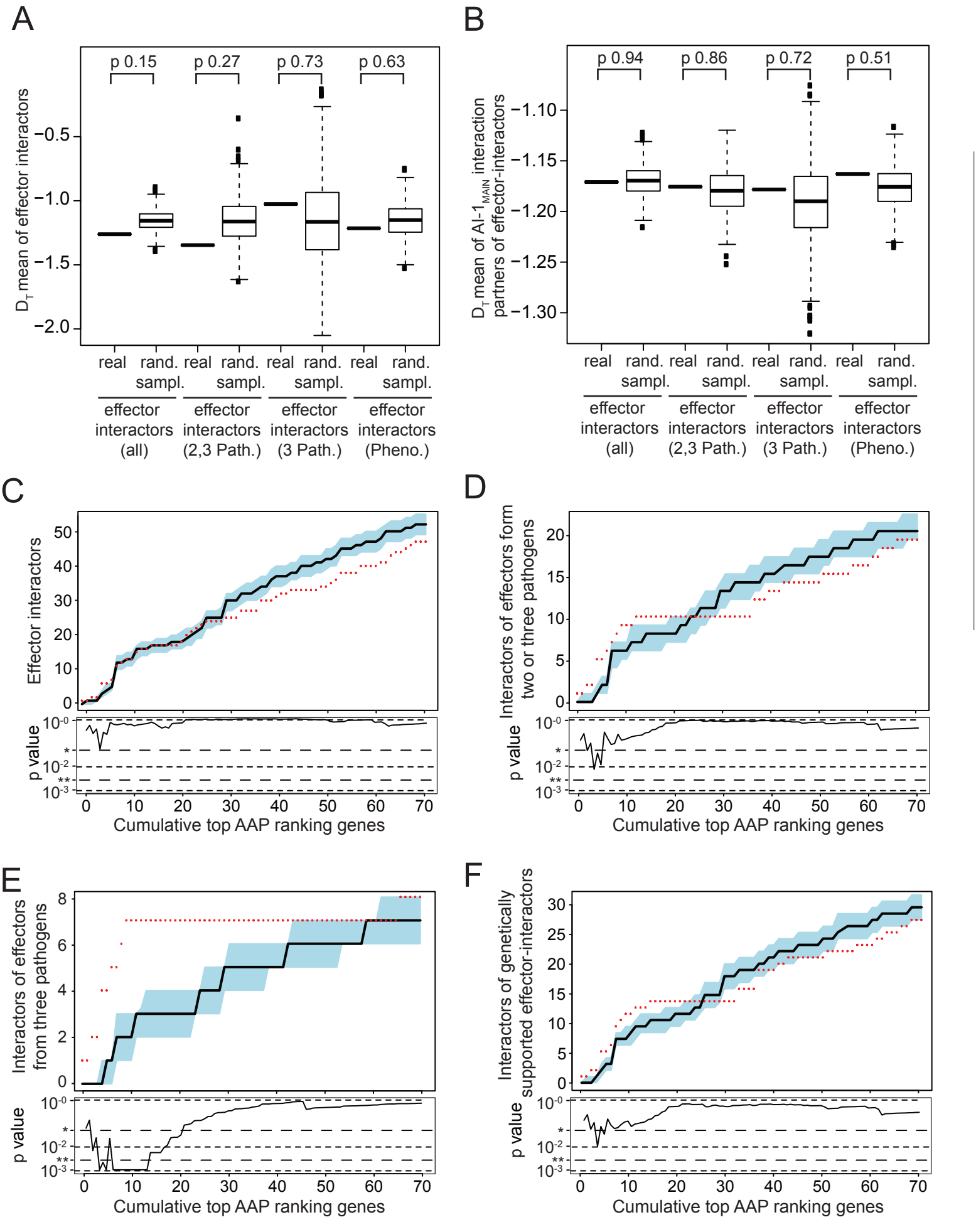

Legends to Supplementary Figures

Figure S1: Datasets and subsets used in the manuscript, related to Figure 1.
A. Graphic representation of the datasets. Names are provided on top of each dataset icon, explanation of the different ORFs used to map the respective datasets are in the legend on top and in the main text.
B. Tabulated summary of different interactions subsets and therein contained effectors, interactions, and interacting host proteins for each pathogen in the 8k, 12k and PPIN-1 search space. 12k and PPIN-1 include the 8k space, respectively. The 8k space interactors that are only in the search space versus those that are also part of the AI-1_{MAIN} network are listed separately.
C. Interactions of OECs, sorted according to phylogenetic relationship, with Arabidopsis host proteins are indicated by blue squares. Grey bars indicate OECs that were not cloned.

Figure S2: Complete plant pathogen interactome network 2 (PPIN-2), related to Figure 2
A. Complete PPIN-2 network contains interactions among host proteins found in PPIN-1, and AI-1_{RPT} and literature curated interactions (LCI).
B. Random network rewiring simulation shows that the effector interacting proteins are less connected than in degree-preserved randomly rewired networks. Shown is the size distribution of the largest connected component formed by the effector-interactors in 10,000 degree-preserved randomly rewired AI-1_{MAIN} networks compared to the observed value (red arrow).

Figure S3: Complete phenotyping data, related to Figure 3.
A. Complete heat-map displaying phenotyping results for all tested T-DNA insertion lines. Locus ID and gene symbol are indicated to the left, IDs of the insertion lines to the right.
B. Comparison of intra- and interspecies convergence. For each Arabidopsis protein interacting with at least two effectors the effector-degree is displayed in a color coded manner as a bar-graph. Arabidopsis proteins only interacting with a single effector are not shown.

Figure S4: TCP14 re-localizes effectors to sub-nuclear foci, related to Figure 4.
A-C. Controls demonstrating that TCP14 did *not* co-localize with controls with which it did not interact in Y2H. These included (**A**) three representative effectors; (**B**) the bZIP5 TF; and (**C**) the unrelated, sub-nuclear body localized PhyB protein. Note that the data in **C** represents images of hypocotyls of two week-old Arabidopsis seedlings hemizygous for 35S:phyB-CFP and EST:TCP14-YFP. Seedlings were grown under white light. To induce the expression of TCP14-YFP, 20µM of estradiol was applied 24 hours before imaging. 20 µM size bars [A-G, top rows] mark the first of three images from the same field. The length of a side of the nuclear images [A-G, bottom rows] is 20 µM.
D. TCP14 does not re-localize *Psy* effectors AvrPto5 and HopBF1.

E. TCP14 re-localizes five additional interacting *Hpa* effectors. HaRXL146 and CRN4b did not co-localize with TCP14-RFP as YFP-tagged fusions, but were re-localized as CFP-tagged fusions by TCP14-YFP.
F,G. TCP14 re-localizes 13 additional interacting *Gor* effectors. All confocal pictures were taken 40-48 hours after infiltration of Agrobacterium strains expressing the different xFP–tagged proteins in leaves of 5-6 week old *N. benthamiana* plants.
H. Western blots of effector fusions used in transient expression assay. Red denotes effectors re-localized to TCP14. Expected molecular masses are given in **Table S4**.

Figure S5: Evolutionary parameters of effectors interactions and high AAP proteins, related to Figure 5
A. For none of the four groups of effector targets is the observed mean D_T significantly different from random expectation. Shown are boxplots of the D_T mean of observed effector-interactors (real) compared to the distribution of means observed in 1,000 random samplings from AI-1_{MAIN} of the same size.
B. For the AI-1_{MAIN} interactors of none of the four groups of effector targets is the observed mean D_T significantly different from random expectation. The boxplots show the D_T mean of observed AI-1_{MAIN} interactors of effector-interactors (real) compared to the distribution of means observed in 1,000 random networks obtained by degree preserving random rewiring. Boxes bracket the 25^{th} and 75^{th} percentile; whiskers indicate the 1.5-fold interquartile distances; dots represent remaining outliers.
C. Real versus randomly observed interacting effector-interactors of top AAP-ranking proteins. Plotted on Y-axis are cumulative counts of effector-interactors interacting with proteins encoded by the top AAP-ranking x genes. Data from AI-1_{MAIN} are shown as red dots, the black line shows the median of 1,000 randomly rewired networks, grey shaded areas show the 25^{th} and 75^{th} percentiles of values found in the rewiring controls. The lower panel provides for each data point the experimentally determined p value (* 0.05; ** 0.005). Boxplots are laid out as in B.
D. Analysis as in B, but counting proteins interacting with effectors from two or three pathogens.
E. Analysis as in B, but counting proteins interacting with effectors from three pathogens.
F. Analysis as in B, but counting proteins interacting with effectors and whose genetic deletion caused an immune phenotype.

Glossary

AAP	Amino Acid Polymorphism – all nucleotide polymorphism that result in a given amino acid change at a specific position in the protein.
AD	GAL4 Activation Domain in the Y2H system
AI-1	Arabidopsis interactome 1, a large-scale interaction network map consisting of AI-1_{MAIN} and AI-1_{RPT}, previously published in Science 2011 (**Figure S1**).
AI-1_{MAIN}	Systematic dataset of the Arabidopsis interactome, obtained by screening 8000 ORFs of the 8k_space systematically against each other twice (**Figure S1**).
AI-1_{RPT}	A dataset obtained by screening a subset of 8k_space, consisting of 1000 x 2000 Proteins against each other 6 times (**Figure S1**).
degree	Number of interaction partners
Effector-degree	Number of virulence effectors interacting with a specific Arabidopsis protein.
EHIn (*Gor*_EHIn, *Hpa*_EHIn, *Psy*_EHIn	Effector Host Interactome – datasets describing interactions between effectors from the investigated (*Psy*, *Hpa*, *Gor*) pathogens with host proteins. Interactions within 8k_space and 12k_space (*Gor* only) and indicated by a respective subscript (**Figure S1**).
DB	GAL4 DNA Binding Domain in the Y2H system
D_T	Tajima's D
edge	Network term for connections between nodes, here: "interactions"
edr	Enhanced disease resistance
eds	Enhanced disease susceptibility
Gor	*Golovinomyces orontii*
Hpa	*Hyaloperonospora arabidopsidis*
node	Network analysis term for connected entities, here proteins
OEC	*G. orontii* effector candidates
ORF	Open Reading Frame
PPIN-1	Plant-Pathogen Interactome Network-1 obtained by screening of Hpa and Psy effectors twice against proteins in the 8k_space and against a selection of immune proteins as described in Mukthar *et al.*, Science, 2011 (**Figure S1**).
Psy	*Pseudomonas syringae*
θ_W	Watterson's estimator θ for the scaled mutation rate
8k_space	8,000 Arabidopsis proteins used to generate AI-1 and PPIN-1
12k_space	12,000 Arabidopsis ORFs, including all of the 8k_space

Supplemental Experimental Procedures

1. Yeast-2-hybrid interactome mapping of OECs

A detailed protocol of the Y2H pipeline used is presented in (Dreze et al., 2010). Briefly, the 84 cloned *OEC*s were transferred into pDest-AD and pDest-DB vectors by Gateway recombination. Successful ORF transfer was confirmed by PCR analysis. Isolated destination clones were transferred into *S. cerevisiae* Y8930 (for DB clones; MATα) and *S. cerevisiae* Y8890 (for AD clones; MATa) by Lithium-Acetate based transformation. Transgenic clones were selected on selective medium and stored in 20% glycerol at -80°C before use. For autoactivator removal, DB- and AD-*OEC* clones were mated with yeast clones containing an empty bait or prey vector on YEPD medium. After o/n incubation, colonies were transferred to selective media for diploid yeast (Sc–Leu–Trp) and incubated o/n. Then, diploid colonies were transferred to interaction media (Sc–Leu–Trp–His + 3-amino-1,2,4-triazole (3-AT), incubated o/n and replica-cleaned (excess yeasts were removed by pushing plates onto a fine velvet on a replica plating block). Three days later, growth phenotypes were scored and autoactivators removed from the *OEC* libraries. The AD-*OEC* yeast clones were pooled by separate growth o/n and unification into one solution. Equal representation of clones in pools was confirmed by plating and colony PCR on 30 colonies. The Arabidopsis library used is described in (Mukhtar et al., 2011); Consortium, 2011). For the screen, single DB-*OEC* clones were mated with pools of 192 AD-At clones, while single DB-At clones were screened against the AD-*OEC* pool. The screen was repeated once. Five µl of freshly grown DB- and AD-yeast were spotted on top of each other on YEPD medium using a robotic fluid handling device. Plates were incubated o/n, colonies replated onto interaction medium as well as cycloheximide (CHX) autoactivator control plates (Sc–Leu–His + 3-AT + CHX (1 mg/l)), incubated o/n and replica-cleaned. After five days incubation, single colonies were isolated and rearrayed into 96-well plates. These primary positive interactors were reevaluated in a secondary screen. They were plated onto diploid-selection medium, incubated two days, and transferred to interaction medium plates (Sc–Leu–Trp–His + 3-AT). Three autoactivator plates (Sc-Leu-His + 1 mM 3-AT + CHX) were also included. Plates were replica-cleaned and incubated three days. Positive clones were restreaked to diploid selection medium, incubated two days and lysed. PCR was used to obtain sequence information on corresponding AD- and DB-clones per colony. The interactors were identified by BLAST searches, single clones of these interactors retrieved from the stock and rearrayed for the retest screen. Matings of single clones were performed as described above, but phenotypes were scored on both Sc–Leu–Trp–His + 3-AT and Sc–Leu–Trp–Ade plates. Interactions were scored as verified when they were positive in three of four repeated matings and autoactivation was never detected.

The experimental methods used to define *Gor*_EHIn were identical to those previously used for mapping bacterial and oomycete effector interactions, and for

producing the Arabidopsis Interactome AI-1 (Consortium, 2011; Mukhtar et al., 2011). Consequently, key parameters of the interactome screen such as sampling- and assay-sensitivity are identical between the experiments and integration of the data will not introduce biases due to experimental design (Venkatesan et al., 2009). Moreover, the 8k_space was systematically tested in all experiments and thus forms a common scaffold for integration. (**Figure S1A**).

2. T-DNA lines and pathogen assays

Homozygous insertion mutants were ordered from ABRC for 124 of 165 effector interactors. Homozygosity and correct insertion sites were verified by PCR using standard conditions. Plants were grown under short day conditions (9 h light, 21°C; 15 h dark, 18°C).

The phenotypic assays have different degrees of difficulty. We funneled the mutant collection through these assays from simplest (*Hpa*), for which we screened 179 mutants and second alleles extensively, to most difficult (*Pto*), where we focused on the mutants that had altered *Hpa* phenotypes and whose products interacted with the most effectors.

Hyaloperonospora arabidopsidis (Hpa) isolates, inoculations, and growth assays. Hpa isolates Emwa1, Emoy2, and Noco2 were propagated on the susceptible Arabidopsis ecotypes Ws-2, Oy-1 and Col-0, respectively (Dangl et al., 1992; Holub et al., 1994). Twelve day old seedlings were inoculated with sporangia suspended in water at a concentration of 30,000 spores/ml. Plants were kept covered with a lid to increase humidity and grown at 21°C with a 9 hrs light period. Sporangiophores were counted on cotyledons at 4 (*Hpa* Noco2) or 5 (*Hpa* Emwa1 and Emoy2) days post-infection (dpi) as described (Holt et al., 2005). The number of sporangiophores per cotyledon was determined on approximately 100 cotyledons / genotype.

Bacterial infection assays. P. syringae pv tomato DC3000 growth assays were performed as previously described (Holt et al., 2005) with modifications. Briefly, bacteria were resuspended in 10 mM $MgCl_2$ to ~$1x10^5$ cfu/ml and syringe infiltrated into leaves of ~5 week old wild type and mutant plants. Leaf discs were cut from the infiltrated area on the day of infiltration (0 dpi) and 3 dpi, and placed into Eppendorff tubes containing 3 glass beads and 400µl 10 mM $MgCl_2$. Tissue was ground using a Fastprep-24 Instrument (MP Biomedicals). Serial dilutions were plated on KB-agar plates and cfu/ml were determined. For day 0 samples, four leaf discs were transferred to the same microfuge tube and processed as described above. For day 3 samples, 8 x 4 leaf discs were processed. The experiment was repeated at least 3 times.

Fungal infection assays. Powdery mildew infections were carried out as described previously, except that spores were harvested at 7 dpi (Weßling et al., 2012). Inoculations were either performed on 18 day old seedlings or 4-5 week old plants. Briefly, inoculations were either performed on three pots per genotpye containing ~200 18 day old seedlings or four 4-5 week old plants were inoculated

in a settling tower with *G. orontii* spores harvested from four leaves 14-21 dpi. Each round of inoculation included nine pots of randomized genotypes, thus all genotypes were included in three separate inoculations. After one minute incubation the pots were returned to the growth chamber. At seven dpi, three times 200 mg (older plants) or 500 mg (seedlings) plant material was harvested across pots and *G. orontii* spores isolated by shaking in water. The number of spores/g fresh weight was determined by counting eight chambers in a hemocytometer.

3. Transient expression in *N. benthamiana*

Agrobacterium-mediated transient expression assay: N. benthamiana plants were grown in a growth chamber equipped with LGM550 Professional LED Grow Light (LED Grow Master Global LLC, USA) at 24°C(day)/20°C (night) under a 16-h light/8-h dark cycle. *A. tumefaciens* strain GV3101 containing protein expression constructs was grown at 28°C with appropriate antibiotics for 18-24 h. Agrobacterium cells were collected by centrifugation at 10,000 RPM for 1 min, and then resuspended in induction solution (10 mM MES (pH 5.6), 10 mM $MgCl_2$, and 150 µM acetosyringone). Cell suspensions were incubated at room temperature for 2 h before infiltration into *N. benthaminana*. For co-infiltration, Agrobacterium strains expressing different proteins were mixed together at the desired final OD_{600} values (effector OD_{600} =1.5; TCP14 OD_{600} =0.05; and p19 (silencing suppressor) expression plasmid OD_{600} = 0.1) and infiltrated into leaves of 5- to 6-week old *N. benthamiana* plants with a 1 ml needleless syringe.

DAPI staining: DAPI (1 µg/ml) was infiltrated into leaves 1 h before confocal imaging.

Estradiol treatment: 20 µM Estradiol in water with 0.004% Silwet L77 was applied to both abaxial and adaxial sides of leaves 6-8 hours before confocal imaging. The treatment was repeated 1 h later.

Confocal Microscopy Imaging: Leaf discs (5 mm diameter) were collected at 40-48 hours after infiltration. Each effector/TCP14 combination was assayed twice. The abaxial sides of three leaf discs from each co-infiltrated leaf were observed with a confocal microscope (LSM 7 DUO; Carl Zeiss). All samples were imaged with a 40x water objective. Between 5 and 15 nuclei were observed in each repetition. The confocal images were edited with Zen 2009 (Zeiss) and Adobe Photoshop CS2. Zen 2009 (Zeiss) and Excel (Microsoft) were used to create histograms. The excitation and detection wave lengths are listed in **Table S5**.

4. Western Blotting

Proteins were isolated in lysis buffer (20 mM HEPES pH 7.5; 13 % Sucrose; 1 mM EDTA; 1 mM Dithiothreitol (DTT); 0.01 % Triton, 1x complete protease inhibitor cocktail (Roche)) from two 0.9 cm leaf discs/experiment using metal beads and a mixer mill (Retsch, Haan, Germany). After addition of 1 volume loading buffer (125 mM Tris-HCl pH 6.8; 5 % sodium dodecyl sulfate (SDS); 25 % glycerol (v/v); 0.025 % bromphenol blue (w/v); 0.2 M DTT), sample were

denaturated for 5 min at 95°C and the supernatant used for gel electrophoresis and western blotting by standard methods. Fusion proteins were detected by anti-GFP (Roche), anti-HA (Roche) and anti-c-myc (Sigma-Aldrich) antibodies according to manufacturer's instructions.

Supplemental Bioinformatic Procedures

5. Convergence analyses

Intraspecies convergence: Significance of intraspecies convergence was determined experimentally based on the experimentally observed number of interacting *A. thaliana* host proteins within Space 8k_sys for effectors from *Hpa*, *Psy*, and *Gor* provided in **Figure S1B**. For each pathogen effector interactors were sampled randomly from a list of AI-1_{MAIN} proteins (not shown) and from a degree preserved list of AI-1_{MAIN} loci (**Figure 2C-E**) (Consortium, 2011) using the "*sample*" command in R. The second analysis is more stringent as it increases the probability of repeatedly picking the more connected proteins and therefore leads to a lower number of nodes expected by chance. The distribution obtained from 10,000 samplings were plotted and compared to the experimentally observed value. The experimental p value was calculated by dividing the number of samplings where the number of common targets is greater or equals the observed number of common targets by the number of samplings performed. If the observed number of targets is not seen in the simulation, the p value is set to < 0.001.

$$\text{observed p} - \text{value} = \frac{\begin{array}{c}\text{number of samplings where number of common targets} \\ \geq \text{observed number of common targets}\end{array}}{\text{number of samplings}}$$

Interspecies convergence statistics: Significance of the convergence of effectors from different pathogens interacting with common host proteins was determined experimentally. The convergence was determined for all possible pathogen combinations based on the numbers of common interaction partners provided in **Figure 2F**. For each pathogen the number of host interaction partners was sampled randomly from a unique list of proteins in AI-1_{MAIN} (Consortium, 2011) using the "sample" command in R with replacement. The observed number of common proteins for each pathogen combination in each of 10,000 samplings was plotted as a background expectation and compared to the experimentally observed value of common interaction partners provided in **Figure 2F**. The experimental p value was calculated by dividing the number of samplings where the number of common targets is greater or equals the observed number of common interactors by the number of samplings performed. If the observed value of common targets is not seen in the simulation, the p value is set to < 0.001.

$$\text{observed p} - \text{value} = \frac{\text{number of samplings where number of common targets} \geq \text{observed number of common targets}}{\text{number of samplings}}$$

6. Gene Ontology (GO) enrichment

We used GO enrichment analysis to test, which functional processes are overrepresented i) among effector interacting proteins, and ii) among the top 55 ranking genes. To this end we performed a GO enrichment analysis using all loci in AI-1_{MAIN} as the background distribution. The analysis is based on GO annotations of TAIR10 (timestamp: 2013-09-03), which we downloaded from the TAIR ftp-server. We removed all annotations with the evidence code "inferred from electronic annotation" (IEA). 17 out of 2661 loci in AI-1_{MAIN} do not have any manually curated GO annotation. For enrichment analysis we used the GOstats package version 2.28.0 (Falcon and Gentleman, 2007). We used the function hyperGTest to perform a hypergeometric test on the GO terms. We used a p value cut-off of 0.005 and “conditional testing”, which means that parent terms are tested without genes, which already have been found to be significant in a children term.

7. Scoring of phenotypic assays

Scoring significant phenotypes: The three pathogens *H. arabidopsidis*, *P. syringae* and *G. orontii* used in our infection assays have different lifestyles and therefore the level of infection of wild-type and mutant plants is assessed using different statistical approaches. Depending on the data collected for each pathogen we used different statistical tests to determine if a T-DNA line shows a significant difference in pathogen infestation in the infection assay compared to the Col-0 control plants.

Values of *G. orontii* experiments of adult plants and seedlings have been derived from hemocytometer counts and represent spores/g fresh weight. A Gaussian generalized linear model was fitted on the data and used for ANOVA analysis (R package “car”)(Fox and Weisberg, 2011). As we have repeated the inoculation experiments up to four times with a T-DNA line and the control line we treat it as a block experiment, where every T-DNA line and the respective control plants of one batch are treated as one block. The block is treated as second factor in our ANOVA analysis beside the first factor of the knocked-out gene. Our data were analyzed as a two-way ANOVA experiment with the factors gene and batch. The Benjamini & Hochberg method (Benjamini and Hochberg, 1995) was applied for multiple testing correction.

P. syringae data are represented as cfu/ml and have the same characteristics like *G. orontii* data and have been analyzed the same way.

H. arabidopsidis isolates Emwa1, Emoy2 and Noco2 data sets were collected as counts of sporangiophores per cotyledon. These data do not satisfy the requirement of ANOVA for normality distribution. This requires the use of a non-parametric test. We used the Kruskal-Wallis test to calculate the p value and corrected the results with Bonferroni multiple testing correction method.

Determination of edr vs. eds phenotypes: To determine if a given insertion mutant shows an *eds* or *edr* phenotype compared to Col-0 accession, we calculated a $\log_2$ fold change.

For each pathogen / pathogen strain *p* the mean value *x* of raw spore / sporangiophores counts for each T-DNA and Col-0 control line were normalized by scaling values between 0 and 1.

$$\text{Normalized}\left(x_{i,p}\right) = \frac{x_{i,p} - X_{min,p}}{X_{max,p} - X_{min,p}}$$

where $x_{i,p}$ is the raw mean value of the pathogen *p* and the value of the tested gene i. $X_{min,p}$ is the minimum value of pathogen *p* and $X_{max,p}$ is the maximum value of pathogen *p*.

The phenotype of the T-DNA line with respect to the Col-0 control plants was evaluated by calculating the fold change of the mean normalized values of all available batches for each T-DNA line. The average fold change of all batches for a given T-DNA line was converted to a $\log_2$ fold change. A $\log_2$ fold change of 0 means same pathogen infestation of T-DNA line and control line, a negative $\log_2$ fold change shows a lower infestation (enhanced disease resistance) and a positive $\log_2$ fold change indicates a higher infestation (enhanced disease susceptibility).

$$fc_{i,p,k} = \frac{\text{Normalized}\ (x^{M}_{i,p,k})}{\text{Normalized}\ (x^{C}_{i,p,k})}$$

$fc_{i,p,k}$ is the fold change of T-DNA line i inoculated with pathogen *p* in batch k. Normalized($x^{M}_{i,p,k}$) is the normalized value of T-DNA line i inoculated with pathogen *p* in batch k and Normalized($x^{C}_{i,p,k}$) is the normalized value of control line of T-DNA line i inoculated with pathogen *p* in batch k.

$$\text{Log}_2 fc_{i,p} = \log_2\left(\frac{fc_{i,p,k}}{n_i}\right)$$

$\text{Log}_2 fc_{i,p}$ is the log2 fold change of T-DNA line i of pathogen *p*. $fc_{i,p,k}$ is divided by the number of batches n_i of the respective T-DNA line i.

Merging phenotypes for multiple T-DNA lines: For the summarized phenotypic analysis of mutants we combined the phenotypic outcome if more than one T-DNA line per gene was available. Therefore we compared the pathogen-specific

p values of the phenotypes on the different T-DNA lines representing the same gene. We selected the phenotypic outcome with the lowest (most significant) p value to obtain merged phenotypes for a gene. We found no contradictory phenotypes for any pathogen, i.e. we had no case where we observed an *edr* phenotype in one mutant line and an *eds* phenotype in the other mutant line. In 15 cases we observed a statistically significant pathogen-specific phenotype in one allele of a gene and no phenotype for the second allele of this gene. In these instances we selected the outcome of the line with the statistically significant result (i.e. the line showing the altered pathogen infection phenotype).

8. Arabidopsis Consensus Sequence Building and AAP evaluation

To evaluate natural variation in Arabidopsis accessions we used the complete genomes of 80 accessions sequenced in the context of the 1001Genomes project and mapped on the Col-0 reference genome. These were collected in eight regions distributed over Europe and Asia, where Arabidopsis naturally occurs and provide a large spatial and phylogenetic distribution adapted in different environments. This dataset was published by Cao et al., 2011 and can be downloaded from 1001genomes.org.

A challenge for the quantitative evaluation of coding variation is the fact that single nucleotide polymorphisms (SNPs) are reported relative to the Columbia (Col-0) reference genome (Cao et al., 2011). This results in numerous SNPs being called in all 80 accessions. In contrast, a conservative nomenclature would identify this as a SNP in Col-0 only. We used a majority voting scheme to define the consensus sequence of the Arabidopsis population consisting of the genomic sequences of Col-0 and the dataset MPICao2010 (Cao et al., 2011), which is available at 1001genomes.org (Altmann *et al.*, in preparation). In this scheme, the most common base at any position defines the consensus sequence and all other variants that occur in the population are counted as variant SNPs where they occur. The codons in coding regions of the consensus sequence of representative gene models as annotated in TAIR10 were compared against the respective codons in the 81 accessions in the genome matrix. In each accession we examined the codons for synonymous SNPs (sSNPs), non-synonymous SNPs (nsSNPs) and the resulting amino acid. A unique amino acid polymorphism (AAP) is defined qualitatively as a specific amino acid substitution at a given position, independent of the frequency of how often the specific substitution was found in the analyzed population. In other words a SNP leading to a hypothetical G->A substitution counts as a single unique AAP independent of how often this amino acid replacement occurred; a substitution resulting in a hypothetical G->T replacement is counted as a second unique AAP. For each protein we counted the unique number of AAPs observed for an individual position. We calculated the sum of unique AAPs per position of a protein, which results in the number of unique AAPs in a protein.

9. Calculation of Tajima's D (D_T) and Watterson's θ (θ_W)

In order to determine D_T and θ_W values for all genes in AI-1_{Main}, we extracted the aligned genomic sequences of all 80 accessions and Col-0 for the respective

representative gene models as fasta file from the whole genome alignment (TAIR10_genome_matrix_2012_03_13.txt.gz) from the dataset MPICao2010 (Cao et al., 2011) (1001genomes.org/projects/MPICao2010/). This information was used to calculate D_T and θ_W using the standard settings in the *compute* program of the *analysis* software package (version 0.8.4) developed by the Thornton lab (Thornton, 2003).

To rank genes for their genetic variation within the 81 accessions, we calculated a combined rank of D_T and θ_W (Dθ-ranking). We sorted all genes in descending order according to their D_T and θ_W values. Subsequently genes were ranked according to the ascending order of the mean rank of these two lists.

10. Statistics of D_T for effector targets and their AI-1_{MAIN} interactors

To determine whether the D_T values of effector-interactors, or that of their AI-1_{MAIN} interaction partners, deviate significantly from the background distribution, we performed sampling and random rewiring analyses for the four effector groups as indicated in the main text (all targets; targets of two or three pathogens; targets of three pathogens; and targets with phenotype).

To evaluate D_T for effector-interactors, we randomly drew without replacement 1,000 samples of the same size as the respective effector group from the unique set of genes encoding proteins in AI-1_{MAIN} as random control. To analyze the significance of D_T of the AI-1_{MAIN} interaction partners of effector-interactors, we generated 1,000 randomized degree-preserved networks and determined the mean D_T of all interaction partners of the respective effector-interactors in the random networks. For each of the four sets of effector-interactors and their AI-1_{MAIN} interaction partners, we calculated a two-sided p value for the observed mean compared to the distribution of the 1,000 mean values of the random controls. We counted the number of occurrences greater equal and lower equal than population mean +/- (population mean - sample mean), and divided it by the number of samples.

11. Statistical evaluation of top Dθ- and AAP-ranking genes with effector-interactors

Dθ-ranking: We investigated whether proteins encoded by top Dθ-ranking genes preferentially interact with effector-interactors. This analysis was performed for interactions with the four different sets of effector targets: all effector targets; proteins interacting with effectors from two or three pathogens; proteins interacting with effectors of three pathogens; and effector targets showing a phenotype in the phenotyping assay.

We performed 100,000 times a degree-preserving random rewiring of the AI-1_{MAIN} network by permuting two interaction partners of two randomly selected edges using the *rewire* function in the *igraph* R package v0.7.0 (Csardi and Nepusz, 2006). This was repeated to generate 1,000 rewired networks. In each random network we counted the number of effector-interactors interacting with

proteins encoded by the cumulative 1 – 70 top Dθ-ranking genes and the analysis was repeated for each class of effector-interactors. The data was used to calculate the experimental p value for the probability of finding the experimentally observed number of interactions between top Dθ-ranking genes with effector-interactors by chance. We calculated an observed p value by dividing the number of observations with a value greater equal than the real number of observation by the number of generated rewired networks.

Amino Acid Polymorphism Effector Interactors Evaluation: To determine, if loci having a high number of AAPs interact more often with effector targets than other loci, we evaluated the AAP in the same way than the combined Dθ ranking. We sorted the loci descending by their number of AAPs and determined the cumulative number of interacting effector-interactors. To calculate a p value we compared the real value against the distribution of number of effector targets from 1,000 rewired networks. p value calculation and network rewiring was conducted as for evaluation of combined ranking of D_T and θ_W.

12. Fisher Exact Contingency Tables

Proteins that are object of intraspecies convergence are also object of interspecies convergence (based on **Figure S2B**)

AI-1_{MAIN} Effector interactors	Intraspecies convergence	no intraspecies convergence	Total
Interspecies convergence	25	7	32
no intraspecies convergence	31	92	123
Total	56	99	**155**

Two-tailed Fisher's exact test: $p < 0.0001$

REFERENCES

Benjamini, Y., and Hochberg, Y. (1995). Controlling the false discovery rate - a practical and powerful approach to multiple testing. Journal of the Royal Statistical Society Series B-Methodological *57*, 289-300.

Cao, J., Schneeberger, K., Ossowski, S., Gunther, T., Bender, S., Fitz, J., Koenig, D., Lanz, C., Stegle, O., Lippert, C.*, et al.* (2011). Whole-genome sequencing of multiple *Arabidopsis thaliana* populations. Nat Genet *43*, 956-963.

Consortium, A.I.M. (2011). Evidence for network evolution in an Arabidopsis interactome map. Science *333*, 601-607.

Csardi, G., and Nepusz, T. (2006). The igraph software package for complex network research. InterJournal *Complex Systems*.

Dangl, J., Holub, E., Debener, T., Lehnackers, H., Ritter, C., and Crute, I. (1992). Genetic definition of loci involved in Arabidopsis-pathogen interactions. In Methods in Arabidopsis Research, C. Koncz, N.-H. Chua, and S. J, eds. (World Scientific), pp. 393-418.

Dreze, M., Monachello, D., Lurin, C., Cusick, M.E., Hill, D.E., Vidal, M., and Braun, P. (2010). High-quality binary interactome mapping. Methods Enzymol *470*, 281-315.

Falcon, S., and Gentleman, R. (2007). Using GOstats to test gene lists for GO term association. Bioinformatics *23*, 257-258.

Fox, J., and Weisberg, S. (2011). An R Companion to Applied Regression (SAGE Publications).

Holt, B.F., 3rd, Belkhadir, Y., and Dangl, J.L. (2005). Antagonistic control of disease resistance protein stability in the plant immune system. Science *309*, 929-932.

Holub, E.B., Beynon, L.J., and Crute, I.R. (1994). Phenotypic and genotypic characterization of interactions between isolates of *Peronospora-parasitica* and accessions of *Arabidopsis-thaliana*. Molecular Plant-Microbe Interactions *7*, 223-239.

Mukhtar, M.S., Carvunis, A.-R., Dreze, M., Epple, P., Steinbrenner, J., Moore, J., Tasan, M., Galli, M., Hao, T., Nishimura, M.T.*, et al.* (2011). Independently evolved virulence effectors converge onto hubs in a plant immune system network. Science *333*, 596-601.

Thornton, K. (2003). Libsequence: a C++ class library for evolutionary genetic analysis. Bioinformatics *19*, 2325-2327.

Venkatesan, K., Rual, J.F., Vazquez, A., Stelzl, U., Lemmens, I., Hirozane-Kishikawa, T., Hao, T., Zenkner, M., Xin, X., Goh, K.I.*, et al.* (2009). An empirical framework for binary interactome mapping. Nat Methods *6*, 83-90.